O-GlcNAcylation reduces phase separation and aggregation of the EWS N-terminal low complexity region

Michael L. Nosella,[†,‡] Maria Tereshchenko,[‡] Iva Pritišanac,[†,‡] P. Andrew Chong,[†] Jeffrey A. Toretsky,[‖] Hyun O. Lee,[‡] Julie D. Forman-Kay*[,†,‡]

[†]Molecular Medicine Program, The Hospital for Sick Children, Toronto, ON M5G 0A4, Canada;

[‡]Department of Biochemistry, University of Toronto, Toronto, ON M5S 1A8, Canada;

[‖]Departments of Oncology and Pediatrics, Georgetown University, Washington, DC 20057, USA.

Keywords: *Biomolecular Condensates, Phase Separation, O-GlcNAc, FET proteins, EWS, low complexity regions*

ABSTRACT: Many membraneless organelles are thought to be biomolecular condensates formed by phase separation of proteins and other biopolymers. Post-translational modifications (PTMs) can impact protein phase separation behavior, although for many PTMs this aspect of their function is unknown. *O*-linked β-D-*N*-acetylglucosaminylation (*O*-GlcNAcylation) is an abundant form of intracellular glycosylation whose roles in regulating biomolecular condensate assembly and dynamics have not been delineated. Using an *in vitro* approach, we found that *O*-GlcNAcylation reduces the phase separation propensity of the EWS *N*-terminal low complexity region (LCR_N) under different conditions, including in the presence of the arginine- and glycine-rich RNA-binding domains (RBD). *O*-GlcNAcylation enhances fluorescence recovery after photobleaching (FRAP) within EWS LCR_N condensates and causes the droplets to exhibit more liquid-like relaxation following fusion. Following extended incubation times, EWS LCR_N+RBD condensates exhibit diminished FRAP, indicating a loss of fluidity, while condensates containing the *O*-GlcNAcylated LCR_N do not. In HeLa cells, EWS is less *O*-GlcNAcylated following *OGT* knockdown and more prone to aggregation based on a filter retardation assay. Relative to the human proteome, *O*-GlcNAcylated proteins are enriched with regions that are predicted to phase separate, suggesting a general role of *O*-GlcNAcylation in regulation of biomolecular condensates.

INTRODUCTION

The intracellular spaces of living cells are organized into sub-compartments, many of which lack an encapsulating lipid membrane. Several of these 'membraneless' compartments are now understood to be condensates formed by phase separation of their constituent biomolecules [1-3]. Phase-separated condensates can provide unique physical and chemical environments which may contribute to the regulation of diverse biological processes. Determining which mechanisms exist to modulate condensate properties is therefore crucial for understanding their functional (or pathological) roles.

Biological polymers such as proteins and nucleic acids undergo phase separation due to cohesive, multivalent intermolecular interactions. The numbers and types of interactions derive from physicochemical sequence properties, which, in the case of proteins, are further enrichened by post-translational modifications (PTMs) [4, 5]. PTMs can impact various aspects of condensates, ranging from composition to larger-scale morphological properties and formation/disassembly kinetics [6-8]. Consistent with a role for PTMs in modulation of phase separation, the numbers of phosphorylation and methylation sites occurring on proteins statistically correlate with their likelihood to phase separate due to interactions involving pi-contacts [9, 10]. While PTMs play important and nuanced roles in regulating biological phase separation, for many PTMs this aspect of their function has remained unexplored.

O-linked β-D-*N*-acetylglucosaminylation ('*O*-GlcNAc'ylation) is a form of glycosylation occurring in the nucleus, mitochondria and cytoplasm of higher eukaryotic cells [11, 12]. Distinct from the often polymeric and structurally complex extracellular glycans, intracellular *O*-GlcNAcylation entails the reversible modification of serine and threonine *O*-hydroxyl groups with a single GlcNAc moiety. In humans and most other metazoa, addition and removal of *O*-GlcNAc are catalyzed by a single pair of enzymes, *O*-GlcNAc transferase (OGT) and *O*-GlcNAc hydrolase (OGA), respectively, which together regulate modification of over a thousand proteins (currently known) with diverse functions [11, 13-18]. Although *O*-GlcNAcylation is enriched in cellular condensates, such as stress granules [19] and DNA damage puncta [20], its roles in regulating the formation and physical properties of these and potentially other condensates are poorly understood.

O-GlcNAcylation has been found to reduce aggregation and affect phase behavior of certain proteins. For example, *O*-GlcNAcylation of the *Drosophila melanogaster* Polyhomeotic protein enables its incorporation into functional

Polycomb repressive complexes by repressing aggregation of its sterile alpha motif domain [21]. *O*-GlcNAcylation of the nuclear pore complex enhances its passivity and selectivity by tempering interactions between FG-Nups which are otherwise prone to aggregation [22]. Furthermore, *O*-GlcNAcylation of alpha-synuclein [23, 24] and tau [25] inhibits their self-association into pathological fibrillar states commonly associated with neurodegenerative disorders.

The connection between phase separation and protein aggregation is highlighted by recent reports of liquid-like condensates preceding (or promoting) aggregate states through liquid-to-solid phase transitions [26-29], particularly in the case of RNA-binding proteins (RBPs) such as FUS [30] and hnRNPA1 [31, 32]. Liquid-to-solid phase transitions often rely on regions of low sequence complexity (LCRs), particularly prion-like domains (PLDs) [30, 33-36], so-called because of their compositional similarities to bona fide yeast prion proteins [37]. Perturbations that affect the strengths and/or numbers of protein-protein interactions can affect whether condensates are biased towards more liquid-like or solid-like material states [30, 38-43]. For example, serine/threonine phosphorylation of the FUS *N*-terminal LCR, which is a PLD, reduces its phase separation propensity as well as its ability to form fibrils by disrupting cohesive cross-beta type interactions between LCR monomers [40, 44]. Conversely, neurodegenerative disease mutations in FUS and hnRNPA2 can enhance the rate of liquid-to-solid phase transitions by increasing the stabilities of fibrillar structures within initially-liquid condensates [30, 38]. Fine-tuning of condensates' physical properties can impact physiological functions as well [45-48]. Defining how PTMs alter particular condensate material properties is therefore of considerable relevance for understanding condensate function and dysfunction.

The Ewing Sarcoma Breakpoint Region 1 (EWS) protein, a member of the FUS-EWS-TAF15 (FET) protein family that has been frequently examined in the phase separation literature [33, 41, 49-53], is known to be *O*-GlcNAcylated *in vivo* [54]. Given that *O*-GlcNAc reduces protein aggregation and that the EWS N-terminal LCR (LCR_N) is a PLD with potential for aggregation, we hypothesized that *O*-GlcNAc could modulate the interactions that drive liquid-liquid phase separation of EWS LCRs. Taking an *in vitro* approach, we found that *O*-GlcNAcylation raises the saturation concentration at which the EWS LCR_N self-assembles into condensates, including in the presence of the *C*-terminal RNA-binding domains (RBD). *O*-GlcNAcylated EWS LCR_N droplets exhibit more liquid-like relaxation and diffusive behavior than unmodified droplets, which behave more like static aggregates. Condensates containing both the EWS LCR_N and RBD lose their rapid internal FRAP over time and *O*-GlcNAcylation prevents this. By silencing OGT expression in HeLa cells, we found that lower *O*-GlcNAcylation levels correlated with increased retention of EWS in a filter retardation assay, suggesting that *O*-GlcNAcylation directly affects EWS solubility in cells as it does *in vitro*. From a bioinformatic analysis, we found that a significantly greater fraction of *O*-GlcNAcylated proteins are predicted to phase separate compared to the human proteome as a whole. Based on our results, we propose that *O*-GlcNAcylation could regulate the fluidity and function of LCR-containing biomolecular condensates *in vivo*.

RESULTS

While all three FET proteins share similar sequence characteristics and cellular localization tendencies, EWS is the sole member shown to be *O*-GlcNAcylated with high stoichiometry *in vivo* [54]. All three FET proteins contain *N*- and *C*-terminal LCRs (Figure 1A) which undergo phase separation in different contexts, though we did not know if both of these regions in EWS are *O*-GlcNAcylated [55]. To test the effect of *O*-GlcNAc on EWS phase separation, we purified the LCR_N (residues 1-264) and *C*-terminal RBD (residues 265-656) and modified them with recombinant, *Homo sapiens* OGT (nucleocytoplasmic isoform, 110kDa [56]) using the sugar donor substrate, uridine 5'-diphospho-*N*-acetylglucosamine (UDP-GlcNAc) (Figure 1B). We used electrospray ionization mass spectrometry coupled to liquid chromatography (ESI LC-MS) to assess *O*-GlcNAcylation stoichiometry following the reactions (Figure S1). Following an overnight *O*-GlcNAcylation reaction, LCR_N spectra displayed a set of peaks with incremental mass differences of ~203 Da consistent with discrete *O*-GlcNAc modification states ranging from 3 to 10 moieties per LCR_N molecule (Figure 1C, S1A, S1B). The same splitting pattern was not achieved with a catalytically-inactive OGT mutant (K842M), demonstrating a lack of modification in the absence of OGT catalysis (Figure S1C). Spectra of the RBD showed negligible changes, indicating that this region is not *O*-GlcNAcylated *in vitro* (Figure S1D). The distribution of *O*-GlcNAc stoichiometries on the LCR_N is consistent with previous reports showing a range of *O*-GlcNAcylation states *in vivo* for EWS [54, 57]. We conclude that only the *N*-terminal portion of the EWS preceding the RBD is subject to *O*-GlcNAcylation *in vitro*.

Like the *N*-terminal LCR of FUS, the EWS LCR_N self-associates into hydrogels and induces sedimentation of the chimeric fusion protein EWS-FLI1 *in vitro* [41, 53], leading us to hypothesize that the EWS LCR_N could also form liquid-like droplets on its own. Addition of the EWS LCR_N (30μM) into buffer solutions at pH 7.5 with 500mM NaCl immediately resulted in the formation of round, micron-sized foci (hereafter termed 'droplets') which were absent at lower salt concentrations (Figure 1D). Droplet formation correlated with increasing NaCl and LCR_N concentrations in a similar manner as the FUS LCR_N [58] (Figure 1E). To test the influence of *O*-GlcNAc on droplet formation, we purified milligram quantities of the *O*-GlcNAcylated EWS LCR_N from a scaled-up OGT reaction (see SI Methods). The *O*-GlcNAcylated LCR_N formed droplets with similar morphologies as the unmodified protein, albeit at higher NaCl and protein concentrations (Figure 1E,F), implying that *O*-GlcNAc lowers the propensity of the EWS LCR_N to phase separate under these conditions. Like the FUS LCR, we also expected EWS LCR_N phase separation to occur at decreasing temperatures in accordance with upper critical solution temperature-type behavior [58]. We found that unmodified LCR_N samples at pH 7.5 in the presence of 100mM NaCl (i.e., below saturating conditions at room temperature) became turbid as the temperature was decreased below ~16°C, indicating droplet formation below this temperature (Figure 1G circle). Increasing the fraction of *O*-GlcNAcylated LCR_N in the samples led to an incremental lowering of the saturation temperature (Figure 1G triangle,

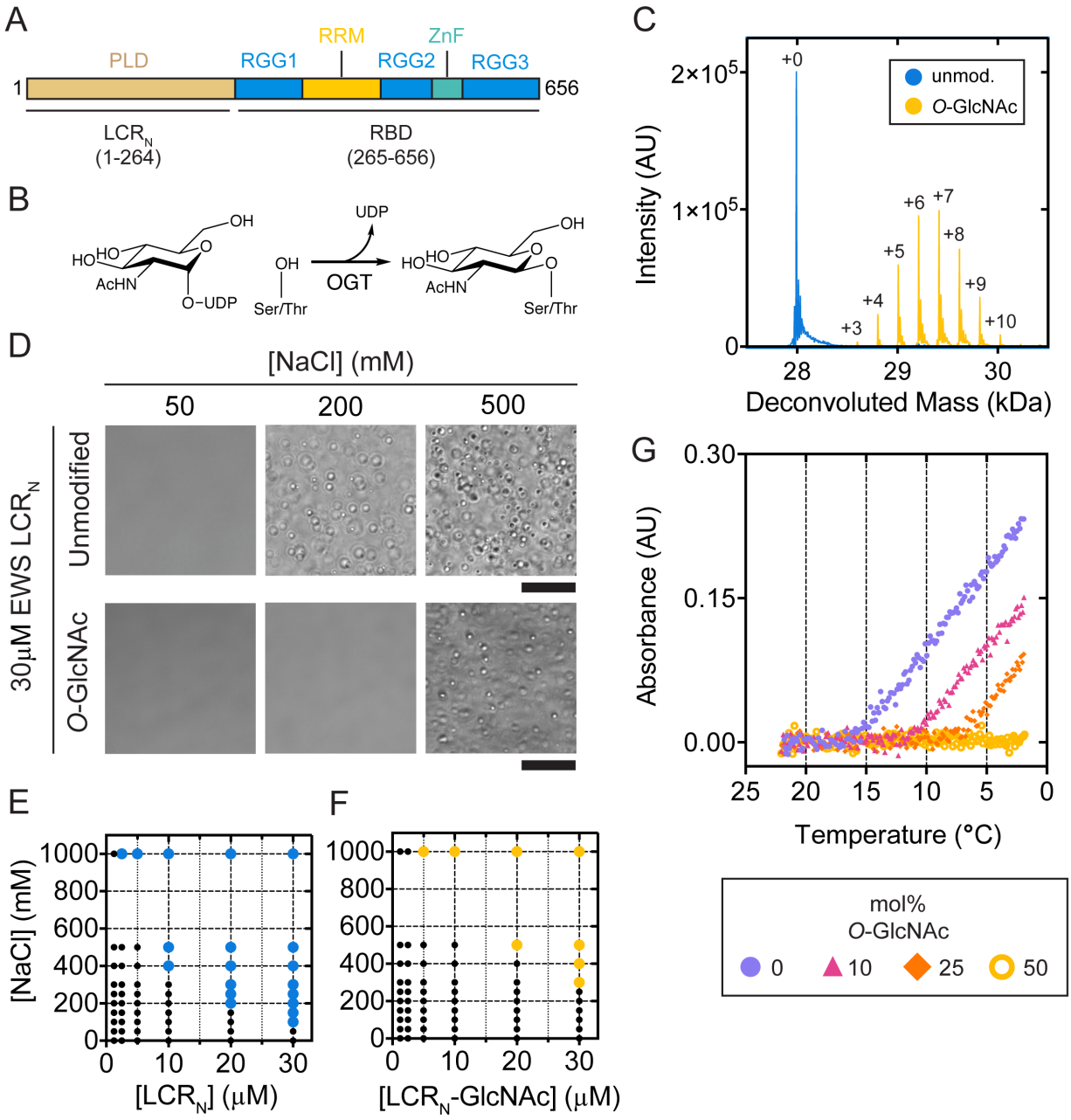

Figure 1. *O*-GlcNAcylation diminishes EWS LCR$_N$ phase separation propensity *in vitro*. (A) Schematic of EWS domain organization. PLD, prion-like domain low-complexity disordered region; RGG, arginine-glycine-glycine rich low-complexity disordered region; RRM, RNA-recognition motif; ZnF, zinc finger. (B) Schematic of the OGT-catalyzed *O*-GlcNAcylation of serine and threonine sidechains. (C) Deconvoluted mass spectra corresponding to unmodified (blue) and *O*-GlcNAcylated (yellow) LCR$_N$. Labels indicate number of *O*-GlcNAc modifications. (D) Differential interference contrast (DIC) micrographs of 30μM unmodified (top) or *O*-GlcNAcylated (bottom) EWS LCR$_N$ in 25mM Tris pH 7.5 at lab temperature with denoted NaCl concentrations. Scale: 20μm. (E,F) Salt and concentration conditions under which (E) unmodified or (F) *O*-GlcNAcylated EWS LCR$_N$ formed droplets. Large, colored dots indicate conditions for which droplets were observed; small black dots indicate an absence of droplets. (G) Temperature-dependent turbidity (λ = 500nm) of LCR$_N$ samples containing variable proportions of *O*-GlcNAcylated LCR$_N$. Total LCR$_N$ concentration is consistently 30μM; legend indicates the proportion of *O*-GlcNAcylated LCR$_N$ present in the samples.

diamond). At a 1:1 ratio of *O*-GlcNAcylated:unmodified LCR$_N$, turbidity was absent at all points of the temperature series under these conditions (Figure 1G ring). Thus, *O*-GlcNAcylation reduces the propensity of EWS LCR$_N$ to phase separate in response to increasing salt concentrations and decreasing temperature.

To determine if phase behavior correlates with the number of *O*-GlcNAc modifications, we prepared small-scale *O*-GlcNAcylation reactions containing the EWS LCR$_N$ and varying concentrations of OGT. Following a 30-minute reaction period, the NaCl concentration was adjusted to 200mM

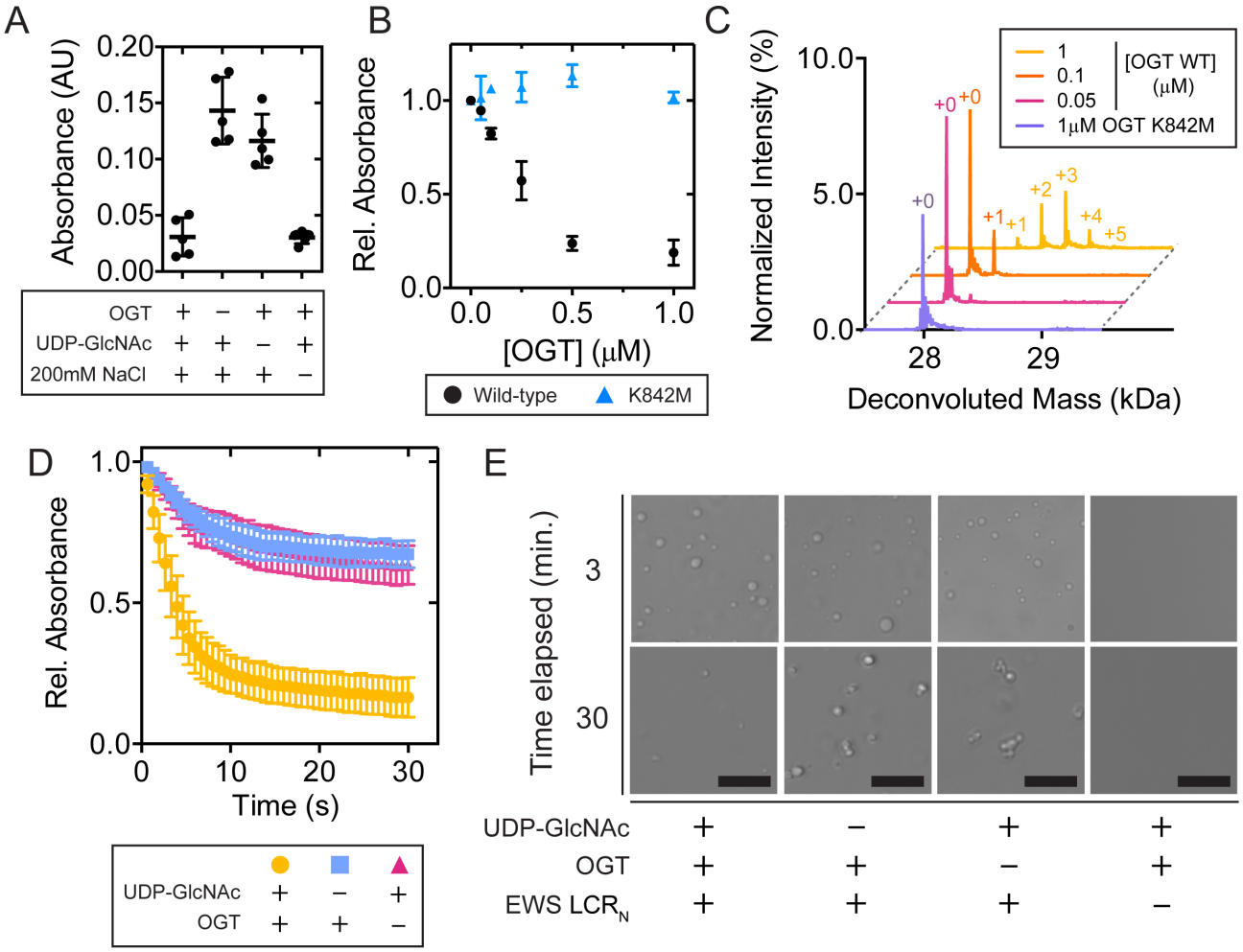

Figure 2. EWS LCR$_N$ phase separation propensity is reduced as *O*-GlcNAc modifications increase. (A) Turbidity (λ = 500nm) of LCR$_N$ (20μM) *O*-GlcNAcylation reaction samples following addition of NaCl. Central bold bars represent mean, with error bars showing standard deviation, n = 5. (B) Relative turbidity (λ = 500nm) of LCR$_N$ (20μM) *O*-GlcNAcylation reactions as a function of varying OGT wild-type (black) or K842M (blue) concentration. Droplet formation was induced by addition of NaCl following a 30-minute reaction period. Error bars represent standard deviation, n = 3. (C) LC-ESI MS analysis of samples in (B). (D) Relative turbidity (λ = 500nm) of LCR$_N$ *O*-GlcNAcylation reactions containing phase-separated EWS LCR$_N$ (20μM) as a function of reaction time. Errors bars represent standard deviation, n = 5. (E) DIC micrographs corresponding to samples in (D) at 3 or 30 minutes post-addition of UDP-GlcNAc. Scale: 20μm. Unless stated otherwise, OGT and UDP-GlcNAc concentrations in each reaction were 1μM and 1mM, respectively.

to promote droplet formation, which we measured by turbidity. EWS LCR$_N$ samples displayed an approximately six-fold increase in turbidity following the addition of NaCl (Figure 2A). Inclusion of both OGT and UDP-GlcNAc resulted in no turbidity change at 30 minutes relative to samples kept at low (50mM) NaCl (Figure 2A). The relative turbidity scaled inversely with the number of *O*-GlcNAc modifications (Figure 2B,C). Substituting wild-type OGT with the catalytically-deficient mutant (K842M) did not produce any changes in turbidity with respect to enzyme concentration (Figure 2B), meaning that the reduction in turbidity seen with wild-type was not merely caused by enzyme binding-induced solubilization of the LCR$_N$. Even the lowest tested OGT concentrations (0.05, 0.1μM) resulted in slight reductions in turbidity, despite only a minor fraction of LCR$_N$ molecules being *O*-GlcNAcylated under these conditions (Figure 2C). These data suggest that *O*-GlcNAcylation lessens salt-induced phase separation of the EWS LCR$_N$ even at sub-stoichiometric modification levels. We then asked whether the LCR$_N$ can be *O*-GlcNAcylated in the condensed phase after phase separation, and if so, will *O*-GlcNAcylation cause the droplets to disassemble. We performed turbidity assays in which LCR$_N$ phase separation was induced with 200mM NaCl prior to the onset of *O*-GlcNAcylation. Following a 30-minute reaction period, LCR$_N$ samples containing OGT and UDP-GlcNAc yielded similar modification patterns to those for reactions performed in the dilute phase (Figure S1E). All samples, including those lacking either OGT or UDP-GlcNAc, displayed time-dependent decreases in turbidity due to the droplets sinking. However, the samples containing both OGT and

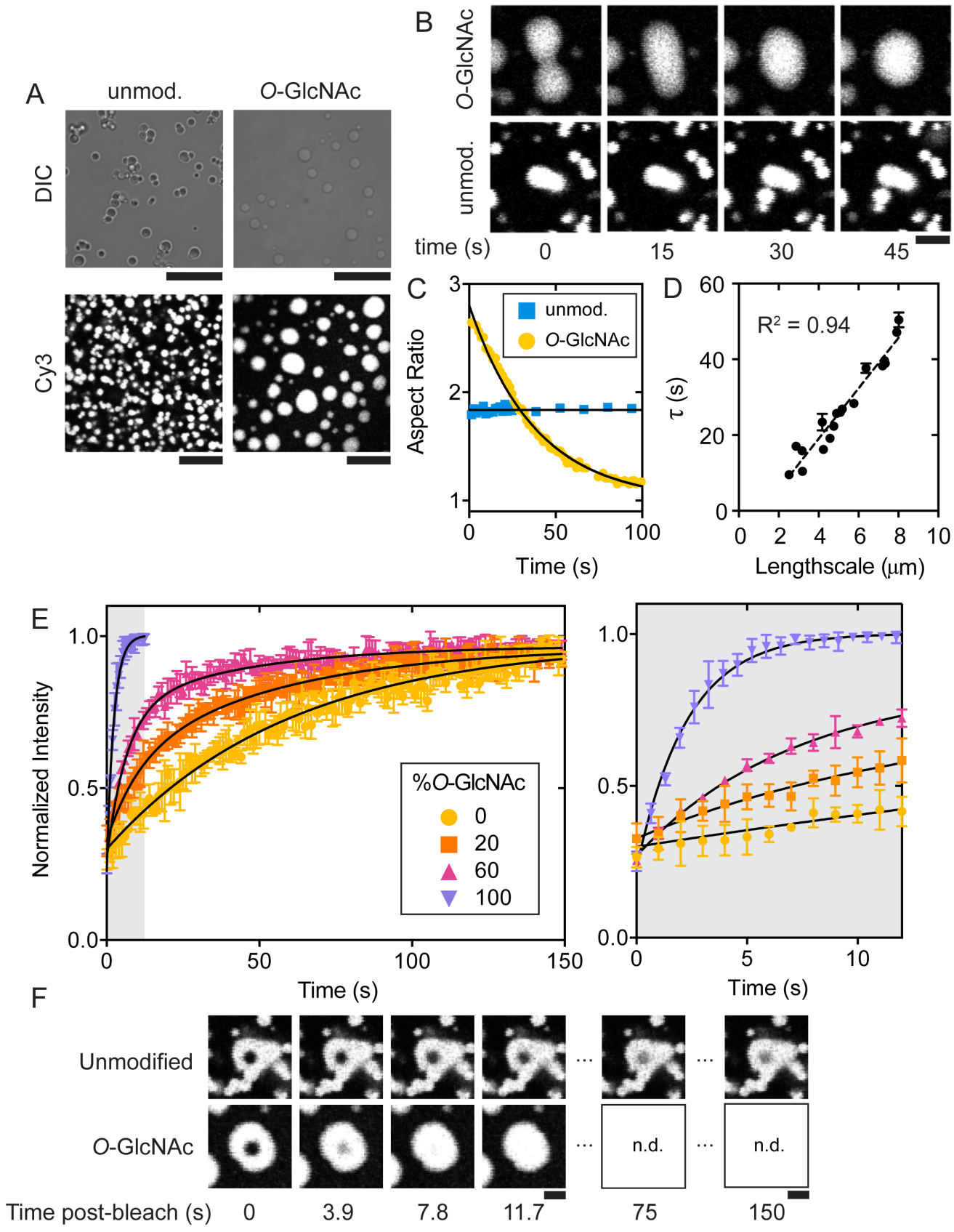

Figure 3. *O*-GlcNAcylation enhances fluidity of EWS LCR$_N$ droplets. (A) DIC and fluorescence micrographs of unmodified (left) or *O*-GlcNAcylated (right) LCR$_N$ droplets. Droplets spiked with 100nM sulfo-Cy3-labelled LCR$_N$ (with or without *O*-GlcNAcylation) were imaged at 30 min. (middle) or 90 min. (bottom) post-formation. Both samples contain 30μM total protein concentration, in 25mM Tris, 500mM NaCl, pH 7.5 at lab temperature. Scale: 20μm. (B) Time lapse images of unmodified (bottom) and *O*-GlcNAcylated (top) sulfo-

Cy3-spiked LCR_N droplets fusing (same conditions as in (A)). Scale: 5μm. (C) Plot of droplet aspect ratio versus time for representative fusion events displayed in (B). (D) Time constants (τ) of exponentially decaying *O*-GlcNAcylated droplet aspect ratio versus length scale (distance between fusing droplets). The slope of the linear fit estimates the inverse capillary velocity (ratio of effective droplet viscosity to surface tension): ~6.6μm s^{-1}. Error bars represent the SEM of fitted τ values. (E) FRAP traces from droplets containing variable ratios of *O*-GlcNAcylated:unmodified EWS LCR_N, spiked with 100nM sulfo-Cy3-labelled LCR_N (with or without *O*-GlcNAcylation). *Right*: Zoom-in of grey shaded area in left panel. N = 4; error bars represent standard deviation. (F) Fluorescence micrographs of representative FRAP time points in (E). n.d.: no data. Scale: 5μm.

UDP-GlcNAc underwent a significantly greater decrease over the 30-minute time course, after which few droplets could be observed by microscopy (Figure 2D,E). Samples lacking either OGT or UDP-GlcNAc contained droplets before and after the reaction period (Figure 2D,E). Interestingly, we never witnessed total clearance of the droplets, perhaps because levels of *O*-GlcNAcylation were generally lower than when the LCR_N was modified in the dilute state (Figure S1E). This could have resulted from the non-mutually exclusive possibilities of OGT having lower catalytic turnover rates in the presence of 200mM NaCl or in the droplets, or from its lower partitioning into the condensed phase. These data demonstrate that *O*-GlcNAcylation can effectively reverse EWS LCR_N droplet formation in vitro.

We then examined how *O*-GlcNAcylation affects the morphologies of EWS LCR_N droplets over time. Within minutes after formation, the unmodified LCR_N droplets cluster into bleb-like structures with irregular boundaries, whereas the *O*-GlcNAcylated droplets merge into larger, circular droplets with smooth boundaries (Figure 3A). To test if the *O*-GlcNAc-dependent morphological differences were caused by changes in the droplets' material properties, we measured the impact of *O*-GlcNAc on droplet fusion, which is a diagnostic characteristic of liquid-like behavior in protein condensates. We prepared samples of the unmodified and *O*-GlcNAcylated LCR_N droplets spiked with 100nM (~0.3mol%) sulfo-cyanine-3 (sulfo-Cy3)-labelled protein for visualization by scanning confocal fluorescence microscopy (Figure 3A). After colliding, *O*-GlcNAcylated droplets spontaneously merged and relaxed into circular shapes when viewed along the xy-plane, tending to a unitary aspect ratio within seconds to minutes (Figure 3B,C). The unmodified droplets adhered upon collision but did not deform, instead retaining their pre-fusion morphologies. For the *O*-GlcNAcylated droplets, the exponential decay in aspect ratio was linearly proportional to the length scale of the fusion event, consistent with previously reported behavior of liquid-like protein condensates in vitro (Figure 3D) [59]. *O*-GlcNAcylated EWS LCR_N droplets fuse more slowly than other in vitro protein condensates such as those formed by NPM1 46, LAF-1 [60] or PR_{60}-repeat peptides with RNA [61], perhaps indicating higher viscosity or surface tension, though the comparison may be skewed by differences in sample conditions.

To determine whether the diffusion of LCR_N molecules within droplets is affected by *O*-GlcNAcylation, we performed fluorescence recovery after photobleaching (FRAP) measurements on the same sulfo-Cy3-spiked droplet samples. Within the unmodified droplets, fluorescence intensity returned to ~90% of pre-bleach levels within a 2.5μm-diameter photobleached region in under 3 minutes (Figure 3E,F), indicating that the majority of molecules remain mobile despite the droplets' inability to fuse. Applying the same photobleaching parameters onto the *O*-GlcNAcylated LCR_N droplets resulted in similar levels of fluorescence recovery on a significantly reduced time scale (Figure 3E,F). Fitting a monophasic exponential model to these data gave fluorescence recovery half-times of 41.6 ± 1.7s and 1.59 ± 0.07s for the unmodified and *O*-GlcNAcylated droplets, respectively. In droplets containing mixed ratios of O-GlcNAcylated and unmodified LCR_N, the recovery half-times decreased proportionally with the amount of *O*-GlcNAcylated LCR_N present (Figure 3E). We cannot confidently estimate diffusion coefficients from these data due to the dissimilar sizes of the differentially modified droplets as well as the potential flaws in using a single-exponential model to describe the underlying diffusion mechanisms [62]. However, the difference in half-times is striking, clearly demonstrating that *O*-GlcNAcylation enhances diffusion of EWS LCR_N molecules within condensates. Based on the disparate fusion behaviors and accelerated FRAP, we suggest that *O*-GlcNAcylation enhances the liquidity of EWS LCR_N droplets, which are otherwise highly viscous or perhaps gel-like in the absence of this modification.

FET protein phase separation is not solely driven by LCR_N self-interactions; rather, the tyrosine-rich LCR_N and arginine-rich RBDs synergistically promote phase separation [9, 50, 63]. Thus, we sought to determine if *O*-GlcNAcylation would impact co-phase separation of these two regions of EWS (Figure 1A). We titrated the EWS LCR_N with or without *O*-GlcNAcylation into samples of the EWS RBD under low-salt buffer conditions in which neither would phase separate on its own. Turbidity increased proportionally with the concentration of unmodified LCR_N and coincided with the presence of droplets (Figure 4A,B). We saw a similar increase as we titrated the *O*-GlcNAcylated LCR_N, however, the onset of turbidity occurred at a higher LCR_N concentration, indicating lower phase separation propensity (Figure 4A,B). This effect was more pronounced when the level of *O*-GlcNAcylation was increased, supporting a direct link between *O*-GlcNAc levels and RBD-dependent droplet formation. As a point of comparison, we also tested the effect of asymmetric dimethylation of the RBD arginines (another PTM shown to mitigate phase separation of FUS [52, 63]) under the same conditions, finding that the increase in saturation concentration was approximately the same as that caused by LCR_N *O*-GlcNAcylation (Figure 4A).

We then tested the effect of LCR_N *O*-GlcNAcylation on the diffusive characteristics of droplets containing both the LCR_N and RBD (LCR_N+RBD droplets), spiked with sulfo-Cy3-LCR_N. Interestingly, the unmodified LCR_N+RBD droplets exhibited more rapid fluorescence recovery than the unmodified LCR_N droplets without addition of the RBD 4C).

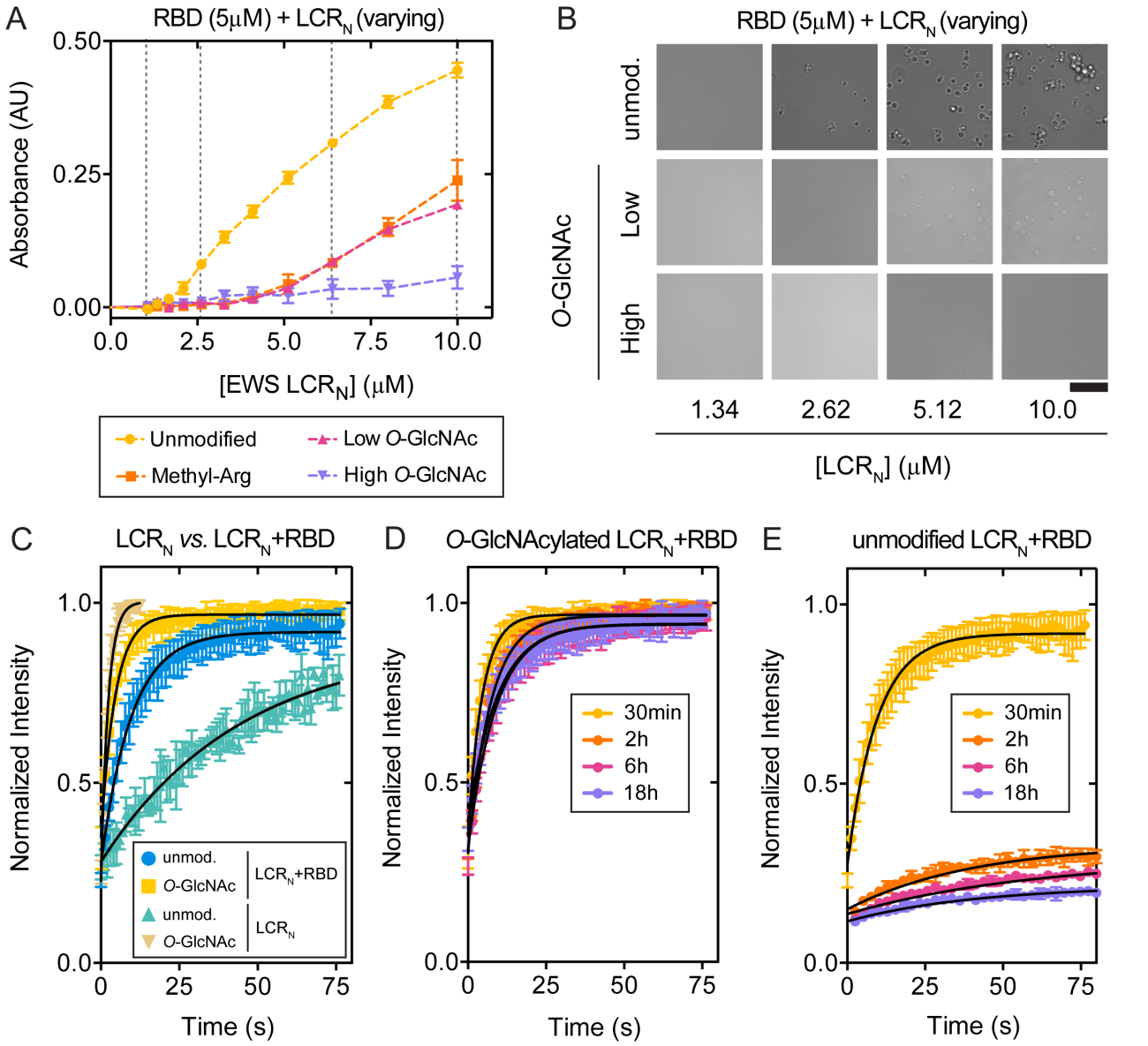

Figure 4. EWS LCR$_N$ *O*-GlcNAcylation reduces RBD-induced phase separation and prevents time-dependent loss of droplet dynamics. (A) Turbidity (λ = 500nm) of EWS RBD samples (5μM; with or without arginine methylation) titrated with LCR$_N$ (with or without *O*-GlcNAcylation) in 25mM Tris, 100mM NaCl, 0.5mM tetrasodium EDTA, 2mM dithiothreitol, pH 7.5 at 25°C. Turbidity was measured immediately after mixing of the two EWS fragments. Error bars represent standard deviation, n = 3. (B) DIC micrographs of samples in (A) indicated by hatched vertical lines. Scale: 20μm. (C) FRAP traces for EWS LCR$_N$ and LCR$_N$+RBD droplets with and without LCR$_N$ *O*-GlcNAcylation. LCR$_N$ droplet samples are the same as in (3E). LCR$_N$+RBD droplet samples contain 10μM LCR$_N$, 100nM sulfo-Cy3-labelled LCR$_N$, 10μM RBD, 25mM Tris, 100mM NaCl, 0.5mM tetrasodium EDTA, 2mM dithiothreitol, pH 7.5 at lab temperature. (D) FRAP traces of *O*-GlcNAcylated and (E) unmodified LCR$_N$+RBD droplets measured at different time points following phase separation under the same conditions as (C). Error bars represent standard deviation, n = 3. Black lines are single exponential fits.

While the FRAP kinetics of the unmodified and *O*-GlcNAcylated LCR$_N$+RBD droplets were similar within 30minutes following phase separation, they began to diverge at later time points (Figure 4D,E). *O*-GlcNAcylated LCR$_N$+RBD droplets exhibited near-complete fluorescence recovery irrespective of the incubation time (Figure 4D,S2), whereas the unmodified droplets already showed decreasing fluorescence recovery at 2 hours post-formation (Figure 4E,S2). The mobile fraction in the unmodified LCR$_N$+RBD droplets decreased even further at later timepoints, reaching only ~10% after 18 hours. These results suggest that molecules within the droplets containing the unmodified LCR$_N$ lose the ability to diffuse in a time-dependent fashion indicating a progression to a less fluid-like material state. *O*-GlcNAcylation prevents this loss of mobility, instead maintaining the liquid-like droplet dynamics that are seen shortly after phase separation.

Based on our observations *in vitro*, we investigated the effect of *O*-GlcNAcylation on EWS aggregation propensity in cells. We used a filter retardation assay (FRA) to monitor EWS aggregation in HeLa cells following changes in *O*-

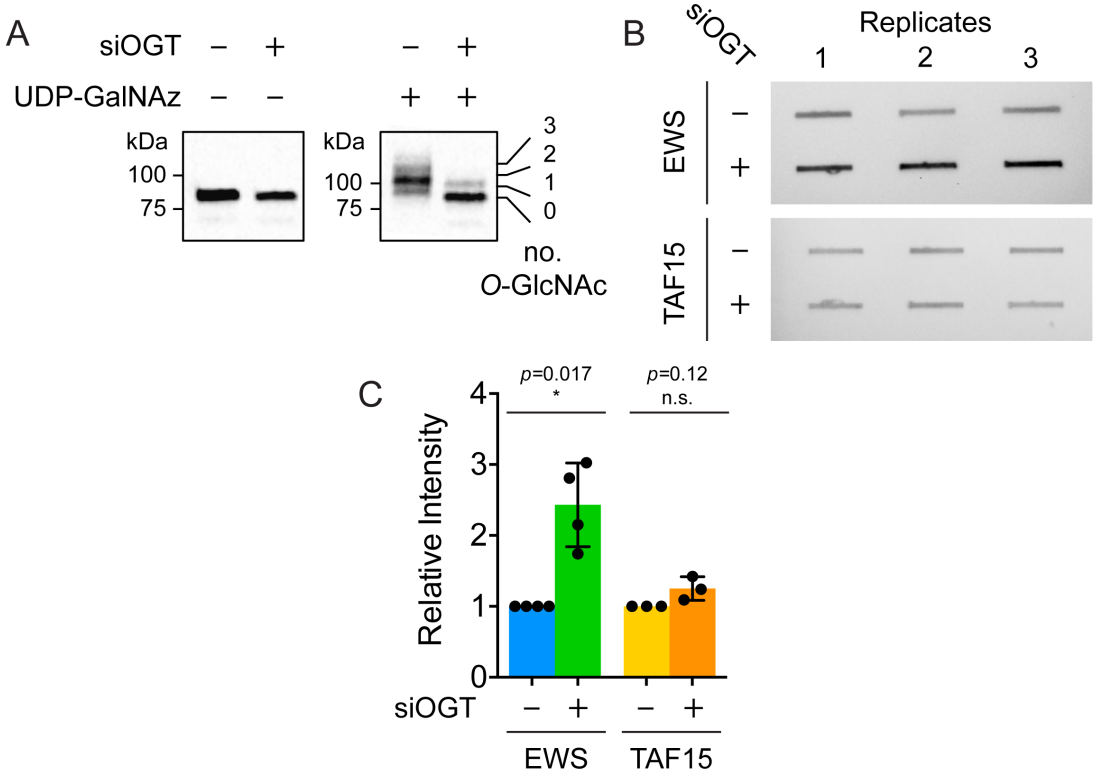

Figure 5. *O*-GlcNAcylation decreases EWS aggregation in HeLa cell lysates. (A) Western blot (anti-EWS) depicting chemoenzymatic (ClickIT) labelling of *O*-GlcNAc moieties on EWS isolated from HeLa cells, treated with or without siOGT (48-hour incubation with 20nM small interfering RNA for OGT). GlcNAc moieties are enzymatically modified with uridine-diphospho-*N*-azidoacetylgalactosamine (UDP-GalNAz) and then alkynyl-PEG (average molecular weight: 5kDa) via Huisgen cycloaddition ('Click' chemistry) to produce an apparent molecular weight shift of ~5kDa per GlcNAc moiety via SDS-PAGE. (B) Representative images of FRA membranes following Western blot detection of EWS (top) or TAF15 (bottom), with and without siOGT treatment. (C) Normalized EWS and TAF15 Western blot intensities from three FRA replicates performed with OGT-depleted HeLa cell lysates. Error bars represent standard deviation. For EWS: $p = 0.017$, Student's *t*-test; n = 4. For TAF15: $p = 0.12$, Student's *t*-test; n = 3.

GlcNAcylation levels. In this assay, large (>0.2μm) sodium dodecyl sulfate (SDS)-insoluble protein aggregates are captured by vacuum filtration on a cellulose-acetate membrane, while smaller protein assemblies and monomers pass through. The captured aggregates are subsequently detected by immunoblotting. To modulate *O*-GlcNAcylation levels, we downregulated OGT expression using small interfering RNA (siOGT), which caused a global reduction in *O*-GlcNAcylation levels (Figure S3A) including reduction in *O*-GlcNAcylation of EWS as measured by chemoenzymatic labeling (Figure 5A). We found that siOGT treatment led to increased EWS aggregation signal in the FRA versus untreated control samples (Figure 5B,C). In contrast, TAF15, another FET family member that is known to phase separate and/or aggregate [36, 50, 64] but is not *O*-GlcNAcylated 54 (Figure S3B), did not experience greater aggregation following siOGT treatment (Figure 5B,C). This suggests that the increased EWS aggregation is a direct consequence of its *O*-GlcNAcylation status rather than a global, protein-nonspecific aggregation caused by decreasing *O*-GlcNAcylation levels. OGT knockdown did not significantly affect the expression levels of EWS or TAF15 (Figure S3C), which could contribute to either protein's aggregation. Taken together, these results show that the aggregation propensity of EWS is directly correlated with its *O*-GlcNAcylation status in cells.

Supposing that *O*-GlcNAcylation might be used by the cell to inhibit aggregation of some phase-separating proteins, we then asked if *O*-GlcNAcylation is generally correlated with higher phase separation propensity. We performed a bioinformatic analysis to calculate the percentage of *O*-GlcNAcylated human proteins predicted to phase separate by three metrics, PScore [9], catGRANULE [65] and PLAAC [66, 67], compared to that for all post-translationally modified proteins included in the PhosphoSitePlus PTM database and the entire human proteome. *O*-GlcNAcylated proteins show a significant enrichment for increased phase separation propensity for each of the three metrics as defined by the fraction scoring above each predictor's preestablished threshold (Figure S4A). To account for differences in the number of proteins above each predictor's cut-off, we also compared the fractions that scored in the top 4th percentile, finding that the enrichment in *O*-GlcNAcylated proteins remains consistent (Figure 6). The significant enrichment also persists across the metrics when querying for proteins with long (>100 residue) IDRs (Figure S4B), indicating that the potentially greater proportion of *O*-GlcNAc site annotations being present in long IDRs and the greater proportion of phase-separating proteins having long IDRs does not affect this finding. These results suggest that phase- separating proteins are more likely to be subject to *O*-GlcNAc-mediated regulation than the proteome in general. PLAAC, which predicts

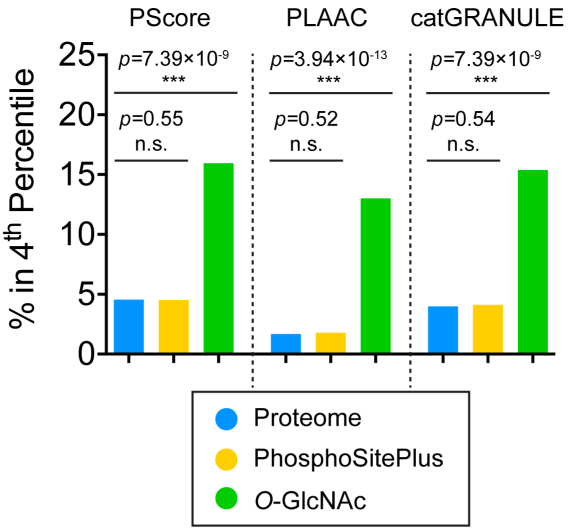

Figure 6. O-GlcNAcylated proteins are enriched for predicted phase separation propensity. Comparison of proteins scoring in the top 4th percentile of the proteome by three different metrics of phase separation propensity (PScore, PLAAC and catGRANULE). Protein sequences for the human proteome were retrieved from the Uniprot database (n = 21047, blue). The human proteins with documented post-translational modifications (n = 19990, yellow) and those modified through *O*-GlcNAcylation (n = 171, green) were retrieved from the PhosphoSitePlus database. The *O*-GlcNAcylated proteins show a significant enrichment for increased phase separation propensity relative to the proteome and post-translationally modified human proteins for each of the three metrics. Indicated *p*-values were derived from Fisher's exact test.

protein regions with prion-like sequence compositional bias [66], showed the greatest statistical enrichment of the three metrics, implying that *O*-GlcNAcylation may be especially relevant for PLD-containing, phase-separating proteins that are prone to aggregation.

DISCUSSION

We examined the effects of *O*-GlcNAc, a widespread PTM with diverse functional consequences [11, 15, 16], on the phase separation and material properties of EWS condensates. *O*-GlcNAcylated LCR_N requires higher protein and salt concentrations and lower temperatures to form droplets, evidence for a decreased phase separation propensity. *O*-GlcNAcylated EWS droplets are more fluid than unmodified droplets based on their increased relaxation to spherical shapes following fusion and their more rapid FRAP. Inclusion of the EWS RBD in trans promotes fluidity at short times, although the internal mobility of LCR_N+RBD droplets diminishes as the unmodified droplets age, perhaps due to a time-dependent increase in PLD-induced cross-beta structure [33]. This transition does not occur when the LCR_N is *O*-GlcNAcylated, suggesting that *O*-GlcNAc preserves fluid-like condensate dynamics over time.

The effects of *O*-GlcNAcylation on the assembly and dynamics of higher-order protein complexes has already been described in several systems, including FG-Nup hydrogels [22], Drosophila Polycomb complexes [21], intermediate filaments [68], and pathological fibrillar aggregates formed by tau and alpha-synuclein [23-25]. In each of these cases, *O*-GlcNAcylation tends to promote protein solubility by sterically disrupting intermolecular interactions between monomers. Our results suggest that the same effect may apply to EWS LCR_N condensates, whose phase separation and liquid-like dynamics are sensitive to the strengths and numbers of *O*-GlcNAc-modulated intermolecular interactions. We demonstrate that *O*-GlcNAc modulates EWS condensate dynamics even at sub-stoichiometric levels, meaning that not all molecules within the condensate must be modified in order for bulk condensate properties to be affected. These results mirror previous findings that sub-stoichiometric *O*-GlcNAcylation slows formation of alpha-synuclein fibrils [23]. Thus, *O*-GlcNAcylation may influence condensate properties even when the modified species are not the most abundant components of the system.

Interactions between tyrosine and arginine residues are significant drivers of phase separation of PLD-containing RNA-binding proteins such as EWS [50]. *O*-GlcNAc reduces phase separation of the tyrosine-rich EWS LCRN together with the arginine-rich RBD, suggesting that it can affect their interactions even though neither of these key residue types [50] are directly modified. The sugar may sterically block cohesive interactions important for phase separation and aggregation, including those underlying cross-beta structures [40]. In addition to these steric effects, *O*-GlcNAc-mediated changes in intermolecular interactions could also derive from bulk changes in the chemical properties of the LCRN. *O*-GlcNAc is uncharged, unlike phosphorylation—to which *O*-GlcNAc is often compared and which is potentially reciprocally regulated [69]. Thus, *O*-GlcNAc weakens LCRN interactions without the benefit of charge-charge repulsion or attraction, which plays a critical role in how phosphorylation disrupts or enhances condensates and fibrils formed by other RNA-binding protein LCRs [40, 41, 44]. Instead, *O*-GlcNAc moieties may disfavour phase separation by altering the hydration properties of the EWS LCR_N [70]. In addition, the *O*-GlcNAc moiety may itself engage in unique intramolecular interactions with the polypeptide chain that compete with the cohesive intermolecular interactions that are important for phase

separation and/or aggregation. Evidence from solid-state NMR studies of *O*-GlcNAcylated FG-Nup hydrogels suggest that such novel sugar-protein interactions do exist and are important for altering the rigidity and secondary structural propensities of FG-Nup molecules within the hydrogel [22].

For several RNA-binding proteins like EWS, phase-separation propensity has been found to correlate with prion-like sequence characteristics [50, 71]. Prions are associated with their propensity to form amyloid fibrillar aggregates that have repetitive cross-beta structure and often exhibit a high resistance to disassembly via chemical or thermal denaturation [72]. Though possessing prion-like sequence characteristics does not necessarily predispose a protein to form such stable structures under physiological conditions, there are a growing number of cases linking the phase separation of PLD-containing proteins with the emergence of fibrillar aggregate states, especially in connection with neurodegenerative disease mutations [30, 33, 38]. It therefore seems probable that cellular mechanisms such as *O*-GlcNAcylation contribute to preventing the aggregation of PLD-containing proteins, particularly in the context of biomolecular condensates in which the nucleation of such aggregates can be promoted by high protein concentrations.

EWS was recently shown to be co-translationally *O*-GlcNAcylated, and is *O*-GlcNAcylated in several different cell lines [54, 55, 57, 73]. These observations suggest that *O*-GlcNAcylation is a constitutive feature of EWS that imparts a persistent regulatory effect on its cellular functions. Our data provide evidence that *O*-GlcNAcylation could be important for regulating EWS aggregation in the context of cellular condensates, which include poly-ADP-ribose-induced DNA damage puncta, paraspeckles and stress granules [64, 74, 75].

EWS *O*-GlcNAcylation was originally discovered in the context of the chimeric fusion protein, EWS-FLI1, in which the C-terminal EWS RBD is swapped for the DNA binding domain of the Friend Leukemia Integration 1 transcription factor (FLI1) due to a chromosomal translocation [55]. EWS-FLI1 is the signature oncogenic transcription factor in Ewing sarcoma family tumors, with the EWS LCR_N acting as a classical activation domain complementing the DNA-binding activity of FLI1. Global inhibition of hexosamine biosynthesis reduces EWS-FLI1 *O*-GlcNAcylation and diminishes the transcriptional output from the EWS-FLI1-targeted Id2 locus in a Ewing Sarcoma cell line [55]. While these results are complicated by the broad off-target effects of hexosamine biosynthesis inhibition, they nevertheless provide compelling initial evidence that *O*-GlcNAcylation affects EWS-FLI1 transcriptional regulation. Recent reports have linked transcription to biomolecular condensates formed by phase separation of transcription factor and coactivator IDRs [76, 77]. EWS-FLI1 has been hypothesized to enhance transcription by forming aberrant condensates on repetitive DNA targets of the FLI1 DNA-binding domain [78], supported by its colocalization to dynamic nuclear 'hubs' containing RNA Pol II [49]. In light of our *in vitro* results, it would be interesting to test if *O*-GlcNAcylation of EWS-FLI1 and other elements of the transcription apparatus, such as the RNA Pol II C-terminal domain (CTD) and TATA-binding protein, affect their partitioning or activity within transcriptional condensates. Indeed, the RNA Pol II CTD and other transcription-associated factors are *O*-GlcNAcylated in the pre-initiation complex and are deglycosylated during elongation [79, 80]. We speculate that, like phosphorylation [81], *O*-GlcNAcylation could regulate the exchange of RNA Pol II and other transcription-associated factors between sequential condensates associated with transcription. Further studies are needed to illuminate the rich regulatory potential of *O*-GlcNAcylation for many biomolecular condensates, including those associated with transcription, DNA repair and stress.

EXPERIMENTAL SECTION

Unless stated otherwise, all chemicals were purchased from BioBasic Canada, Inc. (Markham, ON, Canada).

Plasmids and Cloning. The coding sequence for *Homo sapiens EWSR1*, residues 1-264 (*N*-terminal LCR; LCR_N) was synthesized by GenScript (Piscataway, NJ, USA) with codon optimization for expression in *Escherichia coli*. The LCR_N coding sequence was inserted in frame with a *N*-terminal hexahistidine (His_6)-SUMO tag in a Champion pET SUMO expression vector (Invitrogen, Carlsbad, CA, USA) by Gibson Assembly (New England Biolabs, Ipswich, MA, USA). The coding sequence for EWS 265-656 (the RNA binding domains; RBD) was derived from *H. sapiens EWSR1* cDNA obtained from the NIH Mammalian Gene Collection (MGC), made available through the SickKids SPARC cDNA archive (https://lab.research.sickkids.ca/sparc-drug-discovery/services/molecular-archives/sparc-cdna-archive/). The RBD fragment was amplified via polymerase chain reaction using Kapa HiFi HotStart ReadyMix (Roche, Basel, Switzerland) and then Gibson assembled in frame with an *N*-terminal His_6-SUMO tag in the same vector as above. This construct contains a diglycine insertion at the *N*-terminus of the EWS segment (i.e. directly following the SUMO tag and before residue 265 of EWS).

The pET24b *H. sapiens* ^(nucleocytoplasmic variant, 110kDa) *E. coli* expression plasmid was a kind gift from Suzanne Walker's lab. The K842M mutation was introduced via Site-Directed Mutagenesis using a QuikChange II Kit (Agilent, Santa Clara, CA, USA).

Recombinant Protein Expression. The pET SUMO EWS LCR_N and EWS RBD plasmids were transformed into *E. coli* BL21-CodonPlus (DE3) RIPL chemically competent cells (Agilent). EWS RBD methylation was achieved by co-transformation along with a glutathione *S*-transferase-linked protein arginine methyltransferase 1 (*PRMT1*) *E. coli* expression vector, as previously described [82]. Successful transformants were selected on lysogeny broth (LB)-agar plates containing 50μg mL^{-1} kanamycin sulfate and 34μg mL^{-1} chloramphenicol (also including 100μg mL^{-1} ampicillin in the case of PRMT1 co-expression). Single colonies were used to inoculate ~50mL LB overnight cultures containing the same antibiotics. Following overnight incubation at 37°C with 250rpm shaking, these starter cultures were used to inoculate liter-scale cultures which were then incubated under the same conditions until an optical density at (OD_{600}) of ~1.0 was attained. Recombinant protein expression was initiated by the addition of 0.5mM isopropyl-β-D-thiogalactopyranoside (IPTG). The cultures were then incubated for another ~18 hours at 20°C prior to being harvested

by centrifugation in a JLA9.1000 rotor operating in an Avanti J-26 XP centrifuge (Beckman Coulter, Brea, CA, USA). Cell pellets were suspended in lysis buffer (25mM Tris pH 8.0, 4M guanidinium chloride, 500mM NaCl, 20mM imidazole (Millipore-Sigma Canada, Oakville, ON, Canada), 5mM 2-mercaptoethanol (Millipore-Sigma), pH 8.0) and stored at -20°C until further use.

Protein Purification. Cells were lysed by sonication using a QSonica Q500 sonicator outfitted with a 6mm probe operating at 25% amplitude with 2s pulses / 50% duty for 8 min. total. Lysates were clarified by centrifugation in a JA-20 fixed-angle rotor (Beckman Coulter) operated at 15000 rpm for 1 hour at 4°C. The supernatant was loaded onto a gravity column containing a ~10mL bed volume of Ni Sepharose resin (Cytiva, Marlborough, MA, USA) pre-equilibrated in lysis buffer. After repeated washes with lysis buffer, the bound proteins were eluted with lysis buffer containing 280mM imidazole. These fractions were pooled and dialyzed against ULP buffer (20mM HEPES, 150mM NaCl, 2mM 2-mercaptoethanol) using a 3kDa molecular weight cut-off (MWCO) regenerated cellulose membrane (Spectrum Chemical MFG Co., New Brunswick, NJ, USA). His_6-Ulp1 protease (purified in-house) was then added to cleave the SUMO-tag during overnight dialysis at 4°C. The protease-treated samples were re-loaded over the nickel column to separate the His_6-SUMO tag and protease from the cleaved protein. The flow-through was concentrated using an Amicon 15mL-volume centrifugal concentrator unit equipped with a 3kDa MWCO membrane (EMD-Millipore, Burlington, MA, USA) before being injected onto a Superdex 75 16/600 HiLoad column (Cytiva) pre-equilibrated in size exclusion chromatography (SEC) buffer (25mM Tris, 2M guanidinium chloride, 2mM 2-mercaptoethanol, pH 7.5) on an AKTA FPLC chromatography system (Amersham Biosciences Co., Little Chalfont, UK). Proteins were eluted isocratically at a constant flow rate of 0.5mL min^{-1} with fractions collected every 2 min. Fractions were analyzed by SDS-PAGE with Coomassie staining.

At this stage, the EWS LCR_N was sufficiently pure for further experiments, whereas the RBD required an additional ion exchange purification step to remove excess impurities. The pooled RBD fractions (with or without PRMT1-methylation) were pooled and dialyzed against 25mM HEPES, 50mM NaCl, 0.5mM EDTA, 2mM 2-mercaptoethanol, pH 6.5 in a 3kDa MWCO membrane. The dialyzed sample was clarified by centrifugation at 7000rpm in a fixed-angle Thermo F13 rotor in a Sorvall Legend XFR centrifuge (Thermo Scientific, Waltham, MA, USA) at 4degC for 25 minutes before being loaded onto a 5mL HiTrap sulfopropyl (SP) HP column (Cytiva) pre-equilibrated in the same dialysis buffer as above. After washing the resin with several column volumes of dialysis buffer, the bound protein was eluted over a buffer gradient with increasing NaCl concentration ranging from 50mM to 2M (buffer components were otherwise the same as in the dialysis buffer). Fractions were analyzed by SDS-PAGE; most of the RBD eluted at salt concentrations exceeding 0.5M. The purest fractions were pooled and flash frozen for storage at -80°C.

Wild-type and K842M OGT were purified as previously described [83] with slight modifications. Following the nickel purification, OGT samples were dialyzed against 25mM Tris, 50mM NaCl, 0.5mM EDTA, 2mM dithiothreitol (DTT), pH 7.5 and then concentrated using a centrifugal concentrator equipped with a 50kDa MWCO membrane. Concentrated samples were injected onto a Superdex 200 16/600 HiLoad column (Cytiva) pre-equilibrated in the same dialysis buffer on an AKTA FPLC chromatography system (Amersham Biosciences Co.). The system was run at 4°C with a constant flow rate of 0.5mL min^{-1} with fractions collected every 2min. Fractions were analyzed by SDS-PAGE and Coomassie staining to assess purity. The protein was concentrated to working concentrations of ~20-25μM before being flash frozen and stored at -80°C until further use.

***In vitro O*-GlcNAcylation**. Unless specified otherwise, *O*-GlcNAcylation reactions contained 10μM of the appropriate protein substrate (e.g., EWS LCR_N, RBD), 1μM OGT (wild-type or K842M), 1mM UDP-GlcNAc (Millipore-Sigma), 25mM Tris, 50mM NaCl, 0.5mM EDTA, 2mM dithiothreitol, pH 7.5. The sample volume was scaled according to the quantity of *O*-GlcNAcylated product desired. Analytical- and preparative-scale reactions were incubated for 14 hours at laboratory temperature (~22°C) with gentle rocking. Analytical-scale samples were prepared directly for mass spectrometry at this stage (see below), while preparative-scale samples were quenched by the addition of guanidinium chloride (to 2M final) to facilitate purification by SEC. Concentrated samples were injected onto a Superdex 75 16/600 HiLoad column pre-equilibrated in 25mM Tris, 2M guanidinium chloride, 2mM 2-mercaptoethanol, pH 7.5 on an AKTA FPLC chromatography system. Fractions containing *O*-GlcNAcylated protein were analyzed by SDS-PAGE (a slight migration shift due to *O*-GlcNAcylation was visible as compared to the unmodified protein) and mass spectrometry. The protein was concentrated to ~150μM before being flash frozen and stored at -80°C.

Intact Mass Spectrometry (MS). All MS experiments were conducted at the Structural Genomics Consortium (SGC) Toronto facility. Samples were either prepared directly from analytical-scale *O*-GlcNAc reactions or from preparative-scale purified samples that were first exchanged out of guanidinium chloride-containing buffer into 25mM Tris, pH 7.5. In either case, formic acid was added to a final concentration of 0.1%v/v. 2μL of each sample were injected onto an Agilent UPLC-quadrupolar time of flight (Q-ToF) 6545 MS system equipped with a Dual AJS electrospray ionization source operating in positive ion mode. Samples were desalted online through a C18 column into a mobile phase containing 95%v/v acetonitrile, 4.5%v/v H_2O, 0.5%v/v formic acid. Spectra were recorded over a scan range of 500-3200 m/z at a time interval of 1 scan per second. Raw spectra were processed in Agilent Masshunter software and deconvoluted using the maximum entropy algorithm over a mass range of 10-50kDa with 1Da resolution. Raw and deconvoluted spectra were plotted in GraphPad Prism 6.

Fluorescent Protein Labelling. Aliquots of unmodified or *O*-GlcNAcylated EWS LCR_N were dialyzed in 3.5kDa MWCO GebaFlex midi cassettes (Gene Bio-Applications Ltd., Yavne, Israel) against 25mM sodium phosphate, 2M guanidinium chloride, pH 6.5, to remove the Tris prior to

labelling. Sulfo-cyanine-3 dye conjugated to *N*-hydroxysuccinimide (sulfo-Cy3 NHS-ester; Lumiprobe Co., Hunt Valley, MD, USA) was dissolved in dimethylformamide (Sigma) to a working concentration of 20mM. An appropriate volume of the dye stock was added into a 20μM sample of dialyzed protein to yield a final dye concentration of 200μM. This mixture was allowed to incubate overnight in the dark at 4°C to promote selective labelling of the *N*-terminus. The reaction was quenched by the addition of 25mM Tris, pH 7.5 and filtered through a 0.22μm polyethersulfone membrane (GE Healthcare, Chicago, IL, USA) to remove any aggregates. The filtrate was desalted into 25mM Tris, 2M guanidinium chloride, pH 7.5 using a 5mL HiTrap desalting column (Cytiva) running at a constant flow rate of 1.5mL min^{-1} on an AKTA FPLC system. Fractions containing the labelled protein were analyzed by SDS-PAGE to ensure that fluorescent reaction by-products had been removed. Intact mass spectrometric analysis was also used to confirm labelling. Polyacrylamide gels containing the sulfo-Cy3-modified protein were visualized on a BioRad Chemidoc MP system with Cy3 emission/excitation settings.

Droplet Formation and Microscopy. For all phase separation experiments, EWS LCR_N (with or without *O*-GlcNAcylation or sulfo-Cy3-labelling) was exchanged into 25mM Tris, pH 7.5, by successively concentrating and diluting the protein out of the original guanidinium chloride-containing storage buffer. During this process, the temperature of the centrifuge chamber was set to ≥37°C to limit precipitation which occurred more readily at lower temperature. Droplet formation was induced by combining protein samples 1:1 with buffers containing twice the appropriate NaCl concentration at room temperature. For DIC microscopy, droplet samples were pipetted directly into the wells of 96-well polystyrene glass-bottom plates (Eppendorf, Hamburg, Germany). Images were acquired on a Zeiss Axio Observer 7 microscope with a 40x air objective lens. For fluorescence microscopy, 5μL samples were pipetted into 35mm-diameter uncoated no. 1.5 glass-bottom dishes (MatTek, Ashland, MA, USA) which were subsequently sealed with a glass coverslip to limit evaporation. To enable non-wetting conditions for fusion experiments, the dishes were pre-treated with Sigmacote (Millipore-Sigma) according to the manufacturer's instructions. Fluorescence imaging was performed on a Leica TCS SP8 Lightning / DMi8 system equipped with a Hamamatsu C9100-13 EM-CCD camera. All images were acquired with a 63x oil-immersion objective lens at 1024x1024 pixel resolution. Sulfo-Cy3 fluorescence was detected with a Leica hybrid detector (HyD) following excitation with a 561nm (40mW) laser. Image files were analyzed and processed using Fiji (https://imagej.net/Fiji).

Fluorescence Recovery After Photobleaching (FRAP). FRAP data were collected using the LAS X FRAP module on the same Leica system described above. Circular, 2.5μm-diameter regions of interest (ROI) were positioned in the centres of droplets for bleaching, which was performed in a single pulse at 30% laser power on zoom-in mode. After photobleaching, images were acquired at a frequency of 0.77s^{-1}. Fluorescence intensity measurements from inside the bleached ROI were normalized to measurements from a separate ROI in an adjacent unbleached droplet to correct for passive photobleaching and focus drift. The values were then normalized to the average of 5 pre-bleach scans to yield relative intensity values. The recovery timescale was obtained by fitting a single exponential curve to the processed data: $I(t) = a - be^{-t/\tau}$, where I (t) is relative intensity at each time, t, and a, b and τ are fit parameters. Half-times were calculated as $t_{1/2} = \tau \ln 2$.

Turbidity Assays. Samples were prepared in 96-well clear polystyrene plates prior to being transferred into a 384-well black polystyrene glass-bottom plate (Corning, Corning, NY, USA) for measurement on a SpectriMax i3x plate reader (Molecular Devices, San Jose, CA, USA). The assay buffers typically contained 25mM Tris, 0.5mM EDTA, 2mM DTT, pH 7.5 with a variable NaCl concentrations (to promote or prevent droplet formation) depending on the experimental setup. All sample had a final volume of 15 μL per well. Absorbance measurements were collected at 25 with 500nm-wavelength light at a read-height of 12mm. Data were processed and plotted in GraphPad Prism 6.

Temperature Ramp Experiments. EWS LCR_N (with or without *O*-GlcNAcylation) was dialyzed against 20mM 3-(*N*-morpholino)propanesulfonic acid (MOPS), pH 7.5 in a 3kDa MWCO GebaFlex midi cassettes (Gene Bio-Applications Ltd.) overnight at room temperature. 200μL samples were prepared at 30μM final protein concentration in 20mM MOPS, 150mM NaCl, pH 7.5, with different ratios of unmodified:modified EWS LCR_N present. Samples were pipetted into 250μL 1mm-thick quartz cuvette for turbidity measurements in a JASCO J-1500 circular dichroism spectrophotometer.

Calculating percentages of predicted phase separating proteins. The predictions of phase separation propensities for human proteins were available from Vernon *et al.* [67]. The predictions from three different metrics (catGRANULE [65], PScore [9] and PLAAC [66]) were considered, with method-specific cut-offs used to define propensity to phase separate in a binary manner. A value larger than zero for catGRANULE score was used to define propensity to phase separate. The same cut-off (>0) was used to identify proteins that contain probable prion-like domains by PLAAC. The cut-off of larger or equal than four was used for PScore, as previously established by the authors of the original work. The prediction scores of the three metrics were in addition expressed as a percentage of the human proteome predicted to phase separate in order to unify different scoring schemes across the predictors, with 4% of the human proteome used as a cut-off. The list of sequences of all proteins currently in the PhosphositePlus database was retrieved from the website (https://www.phosphosite.org/Phosphosite_seq.fasta). The set of *O*-GlcNAc modified protein sequences was retrieved from the same database (O-GlcNAc_site_dataset). Both datasets were filtered to include human proteins only. The fractions of the proteins predicted to phase separate in each of the categories: i) proteome; ii) PhosphositePlus; and iii) *O*-GlcNAc, were computed by dividing the number of proteins above the cut-off of each of the metrics (PScore, PLAAC, catGRANULE) by the total number of proteins in each category. A Fisher's exact test was used to assess the signifi-

cance of the difference between the fraction of proteins above the threshold in the human proteome and each of the categories (the *p*-values of the test given in Table S1; and significance indicated with i) '*' $P \leq 0.01$; ii) '**' $P \leq 0.001$; iii) '***' $P \leq 0.0001$).

Defining proteins with long IDRs. SPOT-Disorder [84] was run on the reference human proteome from Uniprot (UP000005640, downloaded on Aug 8, 2019), to obtain a residue-level prediction of intrinsic disorder for all human proteins (canonical sequences only). Short sequences of seven or less residues of predicted 'order' mapped in between long predicted disorder regions were concatenated into the predicted disordered regions. A cut-off of 100 consecutive residues of predicted disorder was used to define 'long IDRs'.

Cell culture and siRNA transfection. Please refer to Table S2 for a detailed list of antibodies used in this study.

HeLa cells were cultured in Dulbecco's Modified Eagle Medium (DMEM) with 10% fetal bovine serum and 1% penicillin-streptomycin. To downregulate expression of *OGT*, cells were reverse-transfected with 20 nM ON-TARGETplus Human *OGT* siRNA (Horizon, cat. no. J-019111-06) for 48 hours using INTERFERin siRNA Transfection Reagent (Polyplus, Illkirch-Graffenstaden, France). Knockdown efficiency was verified by immunoblotting with an anti-OGT antibody (Abcam, Cambridge, UK), while global *O*-GlcNAc levels were assessed by immunoblotting with an anti-*O*-GlcNAc (RL2) antibody (Abcam).

O-GlcNAc stoichiometries on EWS and TAF15 in HeLa cell lysates were measured by Western blotting with the appropriate antibodies (Abcam) after the lysates were processed with the ClickIT *O*-GlcNAc Enzymatic Labelling and ClickIT detection assay kits (Invitrogen). Volumes of lysate containing ~200µg of protein dissolved in FRA buffer (see below) were used for these assays. The manufacturer's instructions were followed, with the exception that the alkyne-biotin detection reagent from the latter kit was replaced with methoxy-PEG-alkyne (average MW ~5kDa; Biochempeg, Watertown, MA, USA), which was present at a final concentration of 5mM during the Click chemistry step. After the final protein precipitation step, the pellets were resuspended in 50µL of 4x Bolt LDS sample buffer (Invitrogen) after vigorous vortexing and heating at 70°C. Samples were diluted four-fold with water before being loaded onto a 4-20% tris-glycine polyacrylamide gel (BioRad, Hercules, CA, USA), approximately ~10µg of protein (i.e., 4µL of undiluted dissolved pellet diluted to 16µL with water) per lane. SDS-PAGE and Western blotting were performed according to standard protocols.

Filter retardation assay (FRA). siRNA-transfected cells were harvested and lysed in FRA lysis buffer (20 mM Tris-HCl pH 7.5, 150 mM NaCl, 1 mM EDTA, 1 mM EGTA, 1% Triton X-100, 1x protease inhibitor cocktail) and protein concentration was quantified using a Pierce 660 assay (Thermo Scientific, cat. no. 22660). 10µg of lysate was loaded onto a methanol-activated 0.2µm cellulose-acetate membrane in a BioRad slot-blot apparatus. The wells of the apparatus were washed prior to and after sample loading using RIPA buffer (50mM Tris-HCl pH 7.5, 150mM NaCl, 1%v/v Triton X-100, 0.5%w/v sodium deoxycholate, 0.1%w/v SDS, 5 mM EDTA, 1x protease inhibitor cocktail). Following sample loading and washes, the cellulose-acetate membrane was fixed in methanol for 5 minutes, washed in tris-buffered saline with 0.1%v/v Tween-20 (TBST) for 5 minutes, and subsequently processed for immunoblotting. In brief, the membrane was blocked in 5%w/v skim milk powder / TBST, incubated in primary antibody (anti-EWS and anti-TAF15; overnight at 4°C), incubated in horseradish peroxidase (HRP)-linked secondary antibody (anti-rabbit IgG; 1 hr at RT), and developed on a ChemiDoc Gel Imaging System using Luminata Crescendo Western HRP Substrate (Sigma, WBLUR0500). Signal intensity was quantified using the Gel Analyzer plugin in ImageJ. Three technical replicates were performed for each experiment. Western blots were performed in parallel to ensure equal loading and levels of expression of the proteins of interest.

ASSOCIATED CONTENT

Supporting Information

Supplementary mass spectrometry data, including raw spectra of unmodified and *O*-GlcNAcylated EWS LCR_N (Figure S1). Fluorescence micrographs to accompany FRAP data from LCR_N+RBD droplets in Fig. 4 (Figure S2). Western blots showing (i) depletion of OGT following siOGT treatment of HeLa cells, (ii) lack of *O*-GlcNAcylation on TAF15 in HeLa cells, (iii) negligible changes in EWS and TAF15 expression levels following siOGT treatment (Figure S3). Supplementary bioinformatics data on differential prediction of phase separation propensity for proteins in the human proteome, including those filtered for containing long (>100 residue) IDRs (Figure S4). Tabulated data corresponding to the bioinformatic analyses presented in Figs. 6 and S4 (Table S1). A listed of antibodies used in this study (Table S2).

The Supporting Information is available free of charge on the ACS Publications website.

AUTHOR INFORMATION

Corresponding Author

* forman@sickkids.ca

Notes

The authors declare no competing financial interest.

Funding Sources

M.N. is funded by an Alexander Graham Bell Canada Graduate Scholarship—Doctoral from the Natural Sciences and Engineering Research Council (NSERC) and M.T. by a Vanier Graduate Scholarship. This work was supported by funding to J.D.F.-K. from the Canadian Institutes for Health Research (CIHR) FDN-148375 and the Canadian Cancer Society, to both J.D.F.-K. and H.O.L. from the Canada Research Chair program, and to H.O.L. from NSERC and University of Toronto's Connaught Fund and Medicine by Design, which receives funding from the Canada First Research Excellence Fund. Additional support was from Children's Cancer Foundation, Inc. as a Force 3 Fellowship (J. A.T.), and the NIH R01CA233619-01A1 (J.A.T.), LCCC CCSG Grant P30 CA051008-16 (Lou Weiner, PI, J.A.T.).

ACKNOWLEDGMENT

We would like to thank the SickKids Imaging Facility for their assistance with the microscopy experiments.

REFERENCES

1. Banani, S. F.; Lee, H. O.; Hyman, A. A.; Rosen, M. K., Biomolecular condensates: organizers of cellular biochemistry. *Nat Rev Mol Cell Biol* **2017,** *18* (5), 285-298.
2. Shin, Y.; Brangwynne, C. P., Liquid phase condensation in cell physiology and disease. *Science* **2017,** *357* (6357).
3. Boeynaems, S.; Alberti, S.; Fawzi, N. L.; Mittag, T.; Polymenidou, M.; Rousseau, F.; Schymkowitz, J.; Shorter, J.; Wolozin, B.; Van Den Bosch, L.; Tompa, P.; Fuxreiter, M., Protein Phase Separation: A New Phase in Cell Biology. *Trends Cell Biol* **2018,** *28* (6), 420-435.
4. Lin, Y. H.; Forman-Kay, J. D.; Chan, H. S., Theories for Sequence-Dependent Phase Behaviors of Biomolecular Condensates. *Biochemistry* **2018,** *57* (17), 2499-2508.
5. Brangwynne, C. P.; Tompa, P.; Pappu, R. V., Polymer physics of intracellular phase transitions. *Nature Physics* **2015,** *11* (11), 899-904.
6. Hofweber, M.; Dormann, D., Friend or foe-Post-translational modifications as regulators of phase separation and RNP granule dynamics. *J Biol Chem* **2019,** *294* (18), 7137-7150.
7. Leung, A. K. L., Poly(ADP-ribose): A Dynamic Trigger for Biomolecular Condensate Formation. *Trends Cell Biol* **2020,** *30* (5), 370-383.
8. Owen, I.; Shewmaker, F., The Role of Post-Translational Modifications in the Phase Transitions of Intrinsically Disordered Proteins. *Int J Mol Sci* **2019,** *20* (21).
9. Vernon, R. M.; Chong, P. A.; Tsang, B.; Kim, T. H.; Bah, A.; Farber, P.; Lin, H.; Forman-Kay, J. D., Pi-Pi contacts are an overlooked protein feature relevant to phase separation. *Elife* **2018,** *7*.
10. Kim, T. H.; Tsang, B.; Vernon, R. M.; Sonenberg, N.; Kay, L. E.; Forman-Kay, J. D., Phospho-dependent phase separation of FMRP and CAPRIN1 recapitulates regulation of translation and deadenylation. *Science* **2019,** *365*, 825-829.
11. Zachara, N.; Akimoto, Y.; Hart, G. W., The O-GlcNAc Modification. In *Essentials of Glycobiology*, rd; Varki, A.; Cummings, R. D.; Esko, J. D.; Stanley, P.; Hart, G. W.; Aebi, M.; Darvill, A. G.; Kinoshita, T.; Packer, N. H.; Prestegard, J. H.; Schnaar, R. L.; Seeberger, P. H., Eds. Cold Spring Harbor (NY), 2015; pp 239-251.
12. Levine, Z. G.; Potter, S. C.; Joiner, C. M.; Fei, G. Q.; Nabet, B.; Sonnett, M.; Zachara, N. E.; Gray, N. S.; Paulo, J. A.; Walker, S., Mammalian cell proliferation requires noncatalytic functions of O-GlcNAc transferase. *Proc Natl Acad Sci U S A* **2021,** *118* (4).
13. Hart, G. W., Nutrient regulation of signaling and transcription. *J Biol Chem* **2019,** *294* (7), 2211-2231.
14. Liu, C.; Li, J., O-GlcNAc: A Sweetheart of the Cell Cycle and DNA Damage Response. *Front Endocrinol (Lausanne)* **2018,** *9*, 415.
15. Yang, X.; Qian, K., Protein O-GlcNAcylation: emerging mechanisms and functions. *Nat Rev Mol Cell Biol* **2017,** *18* (7), 452-465.
16. Ong, Q.; Han, W.; Yang, X., O-GlcNAc as an Integrator of Signaling Pathways. *Front Endocrinol (Lausanne)* **2018,** *9*, 599.
17. Akan, I.; Olivier-Van Stichelen, S.; Bond, M. R.; Hanover, J. A., Nutrient-driven O-GlcNAc in proteostasis and neurodegeneration. *J Neurochem* **2018,** *144* (1), 7-34.
18. Hardiville, S.; Hart, G. W., Nutrient regulation of gene expression by O-GlcNAcylation of chromatin. *Curr Opin Chem Biol* **2016,** *33*, 88-94.
19. Ohn, T.; Kedersha, N.; Hickman, T.; Tisdale, S.; Anderson, P., A functional RNAi screen links O-GlcNAc modification of ribosomal proteins to stress granule and processing body assembly. *Nat Cell Biol* **2008,** *10* (10), 1224-31.
20. Chen, Q.; Yu, X., OGT restrains the expansion of DNA damage signaling. *Nucleic Acids Res* **2016,** *44* (19), 9266-9278.
21. Gambetta, M. C.; Muller, J., O-GlcNAcylation prevents aggregation of the Polycomb group repressor polyhomeotic. *Dev Cell* **2014,** *31* (5), 629-39.
22. Labokha, A. A.; Gradmann, S.; Frey, S.; Hulsmann, B. B.; Urlaub, H.; Baldus, M.; Gorlich, D., Systematic analysis of barrier-forming FG hydrogels from Xenopus nuclear pore complexes. *EMBO J* **2013,** *32* (2), 204-18.
23. Marotta, N. P.; Lin, Y. H.; Lewis, Y. E.; Ambroso, M. R.; Zaro, B. W.; Roth, M. T.; Arnold, D. B.; Langen, R.; Pratt, M. R., O-GlcNAc modification blocks the aggregation and toxicity of the protein alpha-synuclein associated with Parkinson's disease. *Nat Chem* **2015,** *7* (11), 913-20.
24. Lewis, Y. E.; Galesic, A.; Levine, P. M.; De Leon, C. A.; Lamiri, N.; Brennan, C. K.; Pratt, M. R., O-GlcNAcylation of alpha-Synuclein at Serine 87 Reduces Aggregation without Affecting Membrane Binding. *ACS Chem Biol* **2017,** *12* (4), 1020-1027.
25. Yuzwa, S. A.; Shan, X.; Macauley, M. S.; Clark, T.; Skorobogatko, Y.; Vosseller, K.; Vocadlo, D. J., Increasing O-GlcNAc slows neurodegeneration and stabilizes tau against aggregation. *Nat Chem Biol* **2012,** *8* (4), 393-9.

26. Ray, S.; Singh, N.; Kumar, R.; Patel, K.; Pandey, S.; Datta, D.; Mahato, J.; Panigrahi, R.; Navalkar, A.; Mehra, S.; Gadhe, L.; Chatterjee, D.; Sawner, A. S.; Maiti, S.; Bhatia, S.; Gerez, J. A.; Chowdhury, A.; Kumar, A.; Padinhateeri, R.; Riek, R.; Krishnamoorthy, G.; Maji, S. K., alpha-Synuclein aggregation nucleates through liquid-liquid phase separation. *Nat Chem* **2020,** *12* (8), 705-716.

27. Kanaan, N. M.; Hamel, C.; Grabinski, T.; Combs, B., Liquid-liquid phase separation induces pathogenic tau conformations in vitro. *Nat Commun* **2020,** *11* (1), 2809.

28. Wegmann, S.; Eftekharzadeh, B.; Tepper, K.; Zoltowska, K. M.; Bennett, R. E.; Dujardin, S.; Laskowski, P. R.; MacKenzie, D.; Kamath, T.; Commins, C.; Vanderburg, C.; Roe, A. D.; Fan, Z.; Molliex, A. M.; Hernandez-Vega, A.; Muller, D.; Hyman, A. A.; Mandelkow, E.; Taylor, J. P.; Hyman, B. T., Tau protein liquid-liquid phase separation can initiate tau aggregation. *EMBO J* **2018,** *37* (7).

29. Boyko, S.; Surewicz, K.; Surewicz, W. K., Regulatory mechanisms of tau protein fibrillation under the conditions of liquid-liquid phase separation. *Proc Natl Acad Sci U S A* **2020,** *117* (50), 31882-31890.

30. Patel, A.; Lee, H. O.; Jawerth, L.; Maharana, S.; Jahnel, M.; Hein, M. Y.; Stoynov, S.; Mahamid, J.; Saha, S.; Franzmann, T. M.; Pozniakovski, A.; Poser, I.; Maghelli, N.; Royer, L. A.; Weigert, M.; Myers, E. W.; Grill, S.; Drechsel, D.; Hyman, A. A.; Alberti, S., A Liquid-to-Solid Phase Transition of the ALS Protein FUS Accelerated by Disease Mutation. *Cell* **2015,** *162* (5), 1066-77.

31. Molliex, A.; Temirov, J.; Lee, J.; Coughlin, M.; Kanagaraj, A. P.; Kim, H. J.; Mittag, T.; Taylor, J. P., Phase separation by low complexity domains promotes stress granule assembly and drives pathological fibrillization. *Cell* **2015,** *163* (1), 123-33.

32. Lin, Y.; Protter, D. S.; Rosen, M. K.; Parker, R., Formation and Maturation of Phase-Separated Liquid Droplets by RNA-Binding Proteins. *Mol Cell* **2015,** *60* (2), 208-19.

33. Kato, M.; Han, T. W.; Xie, S.; Shi, K.; Du, X.; Wu, L. C.; Mirzaei, H.; Goldsmith, E. J.; Longgood, J.; Pei, J.; Grishin, N. V.; Frantz, D. E.; Schneider, J. W.; Chen, S.; Li, L.; Sawaya, M. R.; Eisenberg, D.; Tycko, R.; McKnight, S. L., Cell-free formation of RNA granules: low complexity sequence domains form dynamic fibers within hydrogels. *Cell* **2012,** *149* (4), 753-67.

34. Hennig, S.; Kong, G.; Mannen, T.; Sadowska, A.; Kobelke, S.; Blythe, A.; Knott, G. J.; Iyer, K. S.; Ho, D.; Newcombe, E. A.; Hosoki, K.; Goshima, N.; Kawaguchi, T.; Hatters, D.; Trinkle-Mulcahy, L.; Hirose, T.; Bond, C. S.; Fox, A. H., Prion-like domains in RNA binding proteins are essential for building subnuclear paraspeckles. *J Cell Biol* **2015,** *210* (4), 529-39.

35. Khan, T.; Kandola, T. S.; Wu, J.; Venkatesan, S.; Ketter, E.; Lange, J. J.; Rodriguez Gama, A.; Box, A.; Unruh, J. R.; Cook, M.; Halfmann, R., Quantifying Nucleation In Vivo Reveals the Physical Basis of Prion-like Phase Behavior. *Mol Cell* **2018,** *71* (1), 155-168 e7.

36. Guo, L.; Kim, H. J.; Wang, H.; Monaghan, J.; Freyermuth, F.; Sung, J. C.; O'Donovan, K.; Fare, C. M.; Diaz, Z.; Singh, N.; Zhang, Z. C.; Coughlin, M.; Sweeny, E. A.; DeSantis, M. E.; Jackrel, M. E.; Rodell, C. B.; Burdick, J. A.; King, O. D.; Gitler, A. D.; Lagier-Tourenne, C.; Pandey, U. B.; Chook, Y. M.; Taylor, J. P.; Shorter, J., Nuclear-Import Receptors Reverse Aberrant Phase Transitions of RNA-Binding Proteins with Prion-like Domains. *Cell* **2018,** *173* (3), 677-692 e20.

37. Franzmann, T. M.; Alberti, S., Prion-like low-complexity sequences: Key regulators of protein solubility and phase behavior. *J Biol Chem* **2019,** *294* (18), 7128-7136.

38. Murray, D. T.; Zhou, X.; Kato, M.; Xiang, S.; Tycko, R.; McKnight, S. L., Structural characterization of the D290V mutation site in hnRNPA2 low-complexity-domain polymers. *Proc Natl Acad Sci U S A* **2018,** *115* (42), E9782-E9791.

39. Conicella, A. E.; Dignon, G. L.; Zerze, G. H.; Schmidt, H. B.; D'Ordine, A. M.; Kim, Y. C.; Rohatgi, R.; Ayala, Y. M.; Mittal, J.; Fawzi, N. L., TDP-43 alpha-helical structure tunes liquid-liquid phase separation and function. *Proc Natl Acad Sci U S A* **2020,** *117* (11), 5883-5894.

40. Murray, D. T.; Kato, M.; Lin, Y.; Thurber, K. R.; Hung, I.; McKnight, S. L.; Tycko, R., Structure of FUS Protein Fibrils and Its Relevance to Self-Assembly and Phase Separation of Low-Complexity Domains. *Cell* **2017,** *171* (3), 615-627 e16.

41. Kwon, I.; Kato, M.; Xiang, S.; Wu, L.; Theodoropoulos, P.; Mirzaei, H.; Han, T.; Xie, S.; Corden, J. L.; McKnight, S. L., Phosphorylation-regulated binding of RNA polymerase II to fibrous polymers of low-complexity domains. *Cell* **2013,** *155* (5), 1049-1060.

42. Wang, A.; Conicella, A. E.; Schmidt, H. B.; Martin, E. W.; Rhoads, S. N.; Reeb, A. N.; Nourse, A.; Ramirez Montero, D.; Ryan, V. H.; Rohatgi, R.; Shewmaker, F.; Naik, M. T.; Mittag, T.; Ayala, Y. M.; Fawzi, N. L., A single N-terminal phosphomimic disrupts TDP-43 polymerization, phase separation, and RNA splicing. *EMBO J* **2018,** *37* (5).

43. Afroz, T.; Hock, E. M.; Ernst, P.; Foglieni, C.; Jambeau, M.; Gilhespy, L. A. B.; Laferriere, F.; Maniecka, Z.; Pluckthun, A.; Mittl, P.; Paganetti, P.; Allain, F. H. T.; Polymenidou, M., Functional and dynamic polymerization of the ALS-linked protein TDP-43 antagonizes its pathologic aggregation. *Nat Commun* **2017,** *8* (1), 45.

44. Monahan, Z.; Ryan, V. H.; Janke, A. M.; Burke, K. A.; Rhoads, S. N.; Zerze, G. H.; O'Meally, R.; Dignon, G. L.; Conicella, A. E.; Zheng, W.; Best, R. B.; Cole, R. N.; Mittal, J.; Shewmaker, F.; Fawzi, N. L., Phosphorylation of the FUS low-complexity domain disrupts phase separation, aggregation, and toxicity. *EMBO J* **2017,** *36* (20), 2951-2967.

45. Franzmann, T. M.; Jahnel, M.; Pozniakovsky, A.; Mahamid, J.; Holehouse, A. S.; Nuske, E.; Richter, D.; Baumeister, W.; Grill, S. W.; Pappu, R. V.; Hyman, A. A.; Alberti, S., Phase separation of a yeast prion protein promotes cellular fitness. *Science* **2018,** *359* (6371).

46. Feric, M.; Vaidya, N.; Harmon, T. S.; Mitrea, D. M.; Zhu, L.; Richardson, T. M.; Kriwacki, R. W.; Pappu, R. V.; Brangwynne, C. P., Coexisting Liquid Phases Underlie Nucleolar Subcompartments. *Cell* **2016,** *165* (7), 1686-1697.

47. Putnam, A.; Cassani, M.; Smith, J.; Seydoux, G., A gel phase promotes condensation of liquid P granules in Caenorhabditis elegans embryos. *Nat Struct Mol Biol* **2019,** *26* (3), 220-226.

48. Kroschwald, S.; Munder, M. C.; Maharana, S.; Franzmann, T. M.; Richter, D.; Ruer, M.; Hyman, A. A.; Alberti, S., Different Material States of Pub1 Condensates Define Distinct Modes of Stress Adaptation and Recovery. *Cell Rep* **2018,** *23* (11), 3327-3339.

49. Chong, S.; Dugast-Darzacq, C.; Liu, Z.; Dong, P.; Dailey, G. M.; Cattoglio, C.; Heckert, A.; Banala, S.; Lavis, L.; Darzacq, X.; Tjian, R., Imaging dynamic and selective low-complexity domain interactions that control gene transcription. *Science* **2018,** *361* (6400).

50. Wang, J.; Choi, J. M.; Holehouse, A. S.; Lee, H. O.; Zhang, X.; Jahnel, M.; Maharana, S.; Lemaitre, R.; Pozniakovsky, A.; Drechsel, D.; Poser, I.; Pappu, R. V.; Alberti, S.; Hyman, A. A., A Molecular Grammar Governing the Driving Forces for Phase Separation of Prion-like RNA Binding Proteins. *Cell* **2018,** *174* (3), 688-699 e16.

51. Maharana, S. W., J.; Papadopoulos, D. K.; Richterm D.; Pozniakovsky, A.; Poser, I.; Bickle, M.; Rizk, S.; Guillen-Boixet, J.; Franzmann, T.; Jahnel, M.; Marrone, L.; Chang, Y.-T.; Sterneckert, J.; Tomancak, T.; Hyman, A. A.; Alberti, S., RNA buffers the phase separation behavior of prion-like RNA binding proteins. *Science* **2018,** *360*, 918-921.

52. Hofweber, M.; Hutten, S.; Bourgeois, B.; Spreitzer, E.; Niedner-Boblenz, A.; Schifferer, M.; Ruepp, M. D.; Simons, M.; Niessing, D.; Madl, T.; Dormann, D., Phase Separation of FUS Is Suppressed by Its Nuclear Import Receptor and Arginine Methylation. *Cell* **2018,** *173* (3), 706-719 e13.

53. Boulay, G.; Sandoval, G. J.; Riggi, N.; Iyer, S.; Buisson, R.; Naigles, B.; Awad, M. E.; Rengarajan, S.; Volorio, A.; McBride, M. J.; Broye, L. C.; Zou, L.; Stamenkovic, I.;

Kadoch, C.; Rivera, M. N., Cancer-Specific Retargeting of BAF Complexes by a Prion-like Domain. *Cell* **2017,** *171* (1), 163-178 e19.

54. Kamemura, K., O-GlcNAc glycosylation stoichiometry of the FET protein family: only EWS is glycosylated with a high stoichiometry. *Biosci Biotechnol Biochem* **2017,** *81* (3), 541-546.

55. Bachmaier, R.; Aryee, D. N.; Jug, G.; Kauer, M.; Kreppel, M.; Lee, K. A.; Kovar, H., O-GlcNAcylation is involved in the transcriptional activity of EWS-FLI1 in Ewing's sarcoma. *Oncogene* **2009,** *28* (9), 1280-4.

56. Hanover, J. A., Yu, S., Lubas, W.B., Shin, S.-H., Ragano-Caracciola, M., Kochran, J., Love, D.C., Mitochondrial and nucleocytoplasmic isoforms of O-linked GlcNAc transferase encoded by a single mammalian gene. *Arch Biochem Biophys* **2003,** *409*, 287-297.

57. Kamemura, K.; Abe, H., The glycosylation stoichiometry of EWS species in neuronal cells. *Biosci Biotechnol Biochem* **2017,** *81* (1), 165-167.

58. Burke, K. A.; Janke, A. M.; Rhine, C. L.; Fawzi, N. L., Residue-by-Residue View of In Vitro FUS Granules that Bind the C-Terminal Domain of RNA Polymerase II. *Mol Cell* **2015,** *60* (2), 231-41.

59. Brangwynne, C. P.; Mitchison, T. J.; Hyman, A. A., Active liquid-like behavior of nucleoli determines their size and shape in Xenopus laevis oocytes. *Proc Natl Acad Sci U S A* **2011,** *108* (11), 4334-9.

60. Elbaum-Garfinkle, S.; Kim, Y.; Szczepaniak, K.; Chen, C. C.; Eckmann, C. R.; Myong, S.; Brangwynne, C. P., The disordered P granule protein LAF-1 drives phase separation into droplets with tunable viscosity and dynamics. *Proc Natl Acad Sci U S A* **2015,** *112* (23), 7189-94.

61. Boeynaems, S.; Holehouse, A. S.; Weinhardt, V.; Kovacs, D.; Van Lindt, J.; Larabell, C.; Van Den Bosch, L.; Das, R.; Tompa, P. S.; Pappu, R. V.; Gitler, A. D., Spontaneous driving forces give rise to protein-RNA condensates with coexisting phases and complex material properties. *Proc Natl Acad Sci U S A* **2019,** *116* (16), 7889-7898.

62. Taylor, N. O.; Wei, M. T.; Stone, H. A.; Brangwynne, C. P., Quantifying Dynamics in Phase-Separated Condensates Using Fluorescence Recovery after Photobleaching. *Biophys J* **2019,** *117* (7), 1285-1300.

63. Qamar, S.; Wang, G.; Randle, S. J.; Ruggeri, F. S.; Varela, J. A.; Lin, J. Q.; Phillips, E. C.; Miyashita, A.; Williams, D.; Strohl, F.; Meadows, W.; Ferry, R.; Dardov, V. J.; Tartaglia, G. G.; Farrer, L. A.; Kaminski Schierle, G. S.; Kaminski, C. F.; Holt, C. E.; Fraser, P. E.; Schmitt-Ulms, G.; Klenerman, D.; Knowles, T.; Vendruscolo, M.; St George-Hyslop, P., FUS Phase Separation Is Modulated by a Molecular Chaperone and Methylation of Arginine Cation-pi Interactions. *Cell* **2018,** *173* (3), 720-734 e15.

64. Altmeyer, M.; Neelsen, K. J.; Teloni, F.; Pozdnyakova, I.; Pellegrino, S.; Grofte, M.; Rask, M. D.; Streicher, W.; Jungmichel, S.; Nielsen, M. L.; Lukas, J., Liquid demixing of intrinsically disordered proteins is seeded by poly(ADP-ribose). *Nat Commun* **2015,** *6*, 8088.

65. Bolognesi, B.; Lorenzo Gotor, N.; Dhar, R.; Cirillo, D.; Baldrighi, M.; Tartaglia, G. G.; Lehner, B., A Concentration-Dependent Liquid Phase Separation Can Cause Toxicity upon Increased Protein Expression. *Cell Rep* **2016,** *16* (1), 222-231.

66. Lancaster, A. K.; Nutter-Upham, A.; Lindquist, S.; King, O. D., PLAAC: a web and command-line application to identify proteins with prion-like amino acid composition. *Bioinformatics* **2014,** *30* (17), 2501-2.

67. Vernon, R. M.; Forman-Kay, J. D., First-generation predictors of biological protein phase separation. *Curr Opin Struct Biol* **2019,** *58*, 88-96.

68. Srikanth, B.; Vaidya, M. M.; Kalraiya, R. D., O-GlcNAcylation determines the solubility, filament organization, and stability of keratins 8 and 18. *J Biol Chem* **2010,** *285* (44), 34062-71.

69. Hart, G. W.; Slawson, C.; Ramirez-Correa, G.; Lagerlof, O., Cross talk between O-GlcNAcylation and phosphorylation: roles in signaling, transcription, and chronic disease. *Annu Rev Biochem* **2011,** *80*, 825-58.

70. Ribeiro, S. S., Samanta, N., Ebbinghaus, S., Marcos, J.C., The synergic effect of water and biomolecules in intracellular phase separation. *Nat Rev Chem* **2019,** *3*, 552-561.

71. Gotor, N. L.; Armaos, A.; Calloni, G.; Torrent Burgas, M.; Vabulas, R. M.; De Groot, N. S.; Tartaglia, G. G., RNA-binding and prion domains: the Yin and Yang of phase separation. *Nucleic Acids Res* **2020,** *48* (17), 9491-9504.

72. Yamaguchi, K. I.; Kuwata, K., Formation and properties of amyloid fibrils of prion protein. *Biophys Rev* **2018,** *10* (2), 517-525.

73. Zhu, Y.; Willems, L. I.; Salas, D.; Cecioni, S.; Wu, W. B.; Foster, L. J.; Vocadlo, D. J., Tandem Bioorthogonal Labeling Uncovers Endogenous Cotranslationally O-GlcNAc Modified Nascent Proteins. *J Am Chem Soc* **2020,** *142* (37), 15729-15739.

74. Schwartz, J. C.; Cech, T. R.; Parker, R. R., Biochemical Properties and Biological Functions of FET Proteins. *Annu Rev Biochem* **2015,** *84*, 355-79.

75. Naganuma, T.; Nakagawa, S.; Tanigawa, A.; Sasaki, Y. F.; Goshima, N.; Hirose, T., Alternative 3′-end processing of long noncoding RNA initiates construction of nuclear paraspeckles. *The EMBO Journal* **2012,** *31* (20), 4020-4034.

76. Sabari, B. R.; Dall'Agnese, A.; Boija, A.; Klein, I. A.; Coffey, E. L.; Shrinivas, K.; Abraham, B. J.; Hannett, N. M.; Zamudio, A. V.; Manteiga, J. C.; Li, C. H.; Guo, Y. E.; Day, D. S.; Schuijers, J.; Vasile, E.; Malik, S.; Hnisz, D.; Lee, T. I.; Cisse, II; Roeder, R. G.; Sharp, P. A.; Chakraborty, A. K.; Young, R. A., Coactivator condensation at super-enhancers links phase separation and gene control. *Science* **2018,** *361* (6400).

77. Boija, A.; Klein, I. A.; Sabari, B. R.; Dall'Agnese, A.; Coffey, E. L.; Zamudio, A. V.; Li, C. H.; Shrinivas, K.; Manteiga, J. C.; Hannett, N. M.; Abraham, B. J.; Afeyan, L. K.; Guo, Y. E.; Rimel, J. K.; Fant, C. B.; Schuijers, J.; Lee, T. I.; Taatjes, D. J.; Young, R. A., Transcription Factors Activate Genes through the Phase-Separation Capacity of Their Activation Domains. *Cell* **2018,** *175* (7), 1842-1855 e16.

78. Toretsky, J. A.; Wright, P. E., Assemblages: functional units formed by cellular phase separation. *J Cell Biol* **2014,** *206* (5), 579-88.

79. Ranuncolo, S. M.; Ghosh, S.; Hanover, J. A.; Hart, G. W.; Lewis, B. A., Evidence of the involvement of O-GlcNAc-modified human RNA polymerase II CTD in transcription in vitro and in vivo. *J Biol Chem* **2012,** *287* (28), 23549-61.

80. Hardiville, S.; Banerjee, P. S.; Selen Alpergin, E. S.; Smith, D. M.; Han, G.; Ma, J.; Talbot, C. C., Jr.; Hu, P.; Wolfgang, M. J.; Hart, G. W., TATA-Box Binding Protein O-GlcNAcylation at T114 Regulates Formation of the B-TFIID Complex and Is Critical for Metabolic Gene Regulation. *Mol Cell* **2020,** *77* (5), 1143-1152 e7.

81. Guo, Y. E.; Manteiga, J. C.; Henninger, J. E.; Sabari, B. R.; Dall'Agnese, A.; Hannett, N. M.; Spille, J. H.; Afeyan, L. K.; Zamudio, A. V.; Shrinivas, K.; Abraham, B. J.; Boija, A.; Decker, T. M.; Rimel, J. K.; Fant, C. B.; Lee, T. I.; Cisse, II; Sharp, P. A.; Taatjes, D. J.; Young, R. A., Pol II phosphorylation regulates a switch between transcriptional and splicing condensates. *Nature* **2019,** *572* (7770), 543-548.

82. Nott, T. J.; Petsalaki, E.; Farber, P.; Jervis, D.; Fussner, E.; Plochowietz, A.; Craggs, T. D.; Bazett-Jones, D. P.; Pawson, T.; Forman-Kay, J. D.; Baldwin, A. J., Phase transition of a disordered nuage protein generates environmentally responsive membraneless organelles. *Mol Cell* **2015,** *57* (5), 936-947.

83. Gross BJ, K. B., Walker S, Discovery of O-GlcNAc transferase inhibitors. *J Am Chem Soc* **2005,** *127*, 14588-14589.

84. Hanson, J.; Yang, Y.; Paliwal, K.; Zhou, Y., Improving protein disorder prediction by deep bidirectional long short-term memory recurrent neural networks. *Bioinformatics* **2017,** *33* (5), 685-692.

Insert Table of Contents artwork here

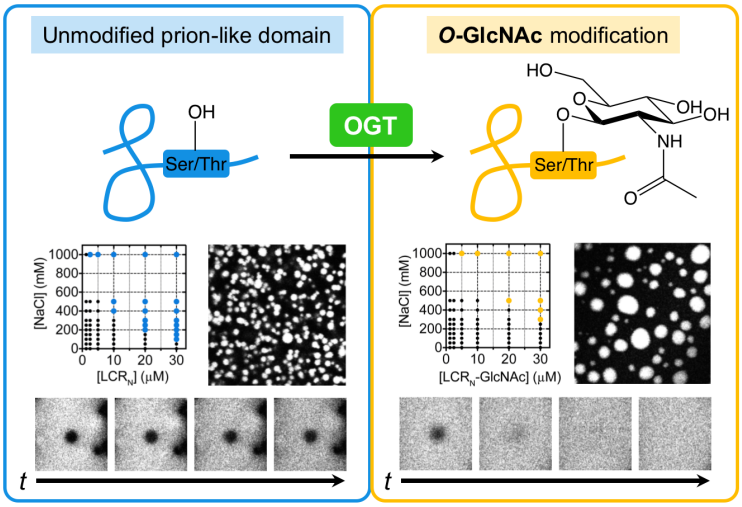

For Table of Contents only.